Novel Multi-Mobility V2X Channel Model in the Presence of Randomly Moving Clusters

Baiping Xiong, Zaichen Zhang, *Senior Member, IEEE*, Jiangfan Zhang, *Member, IEEE*, Hao Jiang, *Member, IEEE*, Jian Dang, *Senior Member, IEEE*, and Liang Wu, *Member, IEEE*

***Abstract*— Considering mobile terminals with time-varying velocities and randomly moving clusters, a novel multi-mobility non-stationary wideband multiple-input multiple-output (MIMO) channel model for future intelligent vehicle-to-everything (V2X) communications is proposed. To describe the non-stationarity of multi-mobility V2X channels, the proposed model employs a time-varying acceleration model and a random walk process to describe the motion of the communication terminals and that of the scattering clusters, respectively. The evolution of the model parameters over time and the stochastic characteristics of the phase shift caused by the time-varying Doppler frequency are derived. The proposed model is sufficiently general and suitable for characterizing various V2X communication scenarios. Under two-dimensional (2D) non-isotropic scattering scenarios, the important channel statistical properties of the proposed model are derived and thoroughly investigated. The impact of the random walk process of the clusters and the velocity variations of the communication terminals on these statistical properties is studied. The simulation results verify that the proposed model is useful for characterizing V2X channels.**

***Index Terms*— Non-stationary V2X channel model, random walk process, velocity variations, time-varying Doppler frequency, statistical properties.**

I. Introduction

THE development of smart cities promotes the deployment of intelligent transportation systems (ITSs). More specifically, as a vital part of intelligent vehicular ad hoc networks, vehicle-to-everything (V2X) communications has been considered a relevant topic in fifth-generation (5G), beyond 5G (B5G), and future sixth-generation (6G) communication systems, which have attracted considerable attention from both industry and academia [1]–[3]. For the development, analysis, and optimization of V2X communication systems, a thorough understanding of the propagation characteristics of the underlying V2X channels is indispensable. This has motivated the development of adequate channel models.

A. Prior Work

In V2X communications, a vehicle can communicate with another moving vehicle (V2V), with stationary roadside infrastructures (V2I), and with slowly moving pedestrians (V2P) via directly established communication links at a dedicated frequency band of 5.9 GHz [1], [2]. The communication terminals are generally equipped with low-elevation antennas, and may also have moving clusters, thus making it totally distinguishable from conventional cellular-based fixed-to-fixed (F2F) [4] and fixed-to-mobile (F2M) [5] channels. To cover all these scenarios, a more general model for V2X channels is necessary. In recent years, various V2V channel models have been studied [6]–[9]. Thus far, different modeling approaches have been introduced for V2X channel modeling, including cluster-based models [10], geometry-based deterministic models (GBDMs) [11], geometry-based stochastic models (GBSMs) [12], [13], non-geometrical stochastic models (NGSMs) [14], [15], and ray tracing models. The deterministic models have high accuracy, but they require a detailed digital map with specific trajectories; moreover, they are computationally expensive. Although NGSMs can achieve relatively low computational complexity, they do not include any geometrical information and cannot be used for system level simulations. GBSMs have a better tradeoff between accuracy and complexity, and can be easily adapted to diverse scenarios by exploiting available geometrical information. Moreover, GBSMs have been widely accepted in standardized protocols [16]–[19]. 3GPP applied a GBSM-based method to develop a three-dimensional (3D) spatial channel model (SCM) for sub-6 GHz band [16] and the frequency band from 0.5 to 100 GHz [17], where the angular/distance/delay parameters can be obtained by exploiting the geometric relationship between the transmitter/receiver and the first/last bounce scatterers. IST defined a GBSM-based non-stationary WINNER II channel model for link and system level simulations [18], where the multipath propagations from the transmitter to the receiver can be determined once the geometric setup is

Manuscript received July 8, 2020; revised November 10, 2020; accepted December 21, 2020. Date of publication January 8, 2021; date of current version May 10, 2021. This work was supported in part by the NSFC Projects under Grant 61960206005, Grant 61971136, Grant 61803211, and Grant 61871111; in part by the Jiangsu NSF Projects under Grant BK20191261 and Grant BK20200820; in part by the Zhejiang Laboratory, under Grant 2019LC0AB02; in part by the Fundamental Research Funds for the Central Universities, Research Fund of National Mobile Communications Research Laboratory; and in part by the Zhishan Youth Scholar Program of SEU. The associate editor coordinating the review of this article and approving it for publication was R. He. *(Corresponding author: Zaichen Zhang.)*

Baiping Xiong, Jian Dang, and Liang Wu are with the National Mobile Communications Research Laboratory, Southeast University, Nanjing 210096, China (e-mail: xiongbp@seu.edu.cn; dangjian@seu.edu.cn; wuliang@seu.edu.cn).

Zaichen Zhang is with the National Mobile Communications Research Laboratory, Southeast University, Nanjing 210096, China, and also with the Purple Mountain Laboratory, Nanjing 211111, China (e-mail: zczhang@seu.edu.cn).

Jiangfan Zhang is with the Department of Electrical and Computer Engineering, Missouri University of Science and Technology, Rolla, MO 65409 USA (e-mail: jiangfanzhang@mst.edu).

Hao Jiang is with the College of Artificial Intelligence, Nanjing University of Information Science and Technology, Nanjing 210044, China, and also with the National Mobile Communications Research Laboratory, Southeast University, Nanjing 210096, China (e-mail: jianghao@nuist.edu.cn).

Color versions of one or more figures in this article are available at https://doi.org/10.1109/TWC.2020.3047957.

Digital Object Identifier 10.1109/TWC.2020.3047957

fixed. Based on the WINNER II channel model [18], ITU-R developed a 3D wideband double direction model, that is, the IMT-Advanced (IMT-A) channel model [19], by specifying the directions of rays. Furthermore, the measurement results in [20] also motivate us to focus mainly on GBSMs.

Owing to the mobility of the communication terminals and clusters in V2X channels, the model parameters and the underlying propagation characteristics can vary rapidly over time. One of the major challenges in the development of high-mobility communications, such as V2X and high speed train (HST) communications, is the acquisition of accurate channel state information (CSI) under complex and fast time-varying scenarios. Moreover, the measurements in [21]–[23] have demonstrated that the wide-sense stationary (WSS) assumption adopted in V2V channel models is only valid within a short time interval, especially for the high-mobility scenarios in future B5G and 6G communications [24]. Therefore, it is of vital importance to consider the non-stationarity in V2X channel modeling.

Cheng *et al.* [25] discussed the present-to-the-near-future work towards intelligent vehicular networks from the aspects of vehicular wireless channels, wireless-vehicle combination, and wireless-vehicle integration. Li *et al.* [14] investigated the frequency domain non-stationarity of an NGSM-based V2V channel model by considering the correlations between the amplitude and phase of different taps. In [15], the non-stationarity in the time domain was studied by using Markov chains to describe multipath component persistence. The authors in [26] proposed a 3D wideband non-stationary GBSM for multiple-input multiple-output (MIMO) V2V channels, where the mobile transmitter (MT) and mobile receiver (MR) were assumed to move in the same direction or in opposite directions. Jiang *et al.* [27] proposed a semi-ellipsoid model to describe the V2V communication channels in tunnel environments, and the impact of arbitrary moving speeds and directions of the vehicles on channel statistical properties were thoroughly investigated. A geometrical-based MIMO channel model for millimeter-wave (mmWave) mobile-to-mobile (M2M) communication environments based on the two-ring reference model is proposed in [28]. However, the models in [26]–[28] only considered the time-varying dynamic channel characteristics induced by the moving transmit and receive vehicles; the scatterers around the transceiver vehicles were assumed to be stationary. By investigating the correlation and spectral properties of the V2V channel, the authors in [29] demonstrated that the presence of moving scatterers can increase the temporal correlation of the channel impulse response and hence result in the non-stationarity of the channel. The authors in [30] studied the impact of moving vehicles around the MT and MR on the underlying propagation characteristics in a narrowband V2V channel. In [31], the authors proposed a non-stationary IMT-Advanced MIMO channel model for high-mobility communication channels, where both the mobile station (MS) and the clusters are in motion.

In general, the aforementioned models used for characterizing V2V channels consider mobile terminals in motion with constant speeds and directions. It is worth mentioning that under real-world conditions, mobile transceivers can experience variations in speeds and directions in different scenarios, which leads to the non-stationarity of channel statistics. The aforementioned models are, therefore, unable to describe scenarios where vehicles experience velocity variations, which, in principle, leads to an inaccurate description of realistic V2X channels. Thus far, only a few studies have investigated the impact of the velocity variations of mobile transceivers. Rauf in [32] proposed a two-dimensional (2D) Rayleigh fading model, in which the transmitter remained stationary and the receiver moved in a constant direction with time-varying speed. Li *et al.* [33] proposed a novel non-stationary model for single-antenna vehicular channels, which considered the velocity variations of both terminals and moving scatterers in different segments. In [34], the authors incorporated the impact of the velocity variations of the MS in a non-stationary multipath channel model; however, they used a narrowband model that only considered the motion of the MS. Subsequently, the authors in [35] extended the model in [34] to a 3D non-stationary wideband MIMO channel model. Nevertheless, in [35], the impact of the motion of the transmitter on channel statistic properties was not studied. The authors in [36] presented a non-stationary channel model based on the two-ring model for M2M scenarios, in which both the variations in the velocity and the trajectory of the transmitter/receiver were considered. However, in [36], the model was dedicated to narrowband single-antenna systems and the impact of moving clusters on channel statistic properties was not investigated. By considering the moving scatterers and velocity variations of the terminals, a closed-form expression of the temporal correlation property of a non-stationary V2V channel model was derived and analyzed in [37]. Overall, the aforementioned channel models mainly adopt over-simplified mobility trajectories to describe the motion of the terminals and the cluster mobility model is not well considered, which will, in principle, lead to inaccurate analysis of channel statistical properties. Therefore, these channel models cannot efficiently describe the non-stationarity in realistic V2X communication scenarios, especially for complicated conditions such as S-shaped paths, crossroads, and time-varying traffic.

B. Motivations

The aforementioned channel models are mainly designed for specific rather than general scenarios, which will, in principle, lead to their relatively low accuracy in describing realistic V2X communication channels. In general, V2X channels can exhibit different properties in different scenarios, and the non-stationary properties have not been sufficiently investigated in the existing channel models because of the use of over-simplified mobility models. This motivates us to study the non-stationarity of the V2X channels in greater depth and propose more general channel models to effectively describe realistic V2X communication scenarios.

C. Main Contributions

In this paper, we propose a general wideband non-stationary MIMO channel model for V2X communications. The main contributions of this study are summarized below:

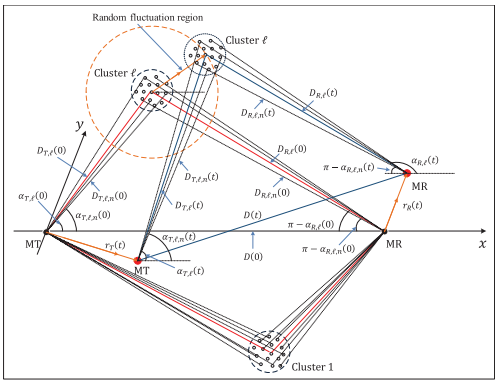

Fig. 1. Illustration of the system parameters of the proposed multi-mobility V2X channel model.

- We propose a novel general non-stationary wideband MIMO GBSM with time-varying model parameters for future intelligent V2X communications in the presence of randomly moving clusters. The proposed GBSM is helpful in describing different V2X communication scenarios by appropriately adjusting the model parameters.
- Unlike conventional V2X channel models, the proposed novel GBSM considers a time-varying acceleration model to describe the velocity and trajectory variations of the mobile terminals. This means that the terminals can move with not only time-varying speeds and trajectories but also with time-varying speed and angular accelerations, thus making the proposed model a more general and realistic description of the movements of the MT and MR, especially for complicated scenarios such as S-shaped paths, crossroads, and time-varying traffic. Moreover, the proposed model can be adapted for different scenarios requiring V2X communications, such as M2M with constant moving, F2M, F2F, etc.
- Considering the non-stationarity caused by the moving clusters, we adopt a random walk process to describe the movements of the clusters. This introduces an additional dimension of randomness to the V2X channel, which has a significant impact on channel non-stationarity. Under this condition, we find that the Doppler phase shift follows a Gaussian random process.

The remainder of this paper is organized as follows. Section II presents the system model, where a novel non-stationary V2X channel model with randomly moving clusters, which follow random walk processes, is proposed. In Section III, the important statistical properties of the proposed V2X channel model are derived and analyzed. The simulation results and discussion are presented in Section IV. Finally, our conclusions are presented in Section V.

II. System Model

A geometrical description of the proposed non-stationary multi-mobility V2X channel model is presented in Fig. 1. In this study, we consider single reflection clusters and neglect multiple reflections because of their very large reflection loss [13]. Then, the signals transmitted by the MT experience single reflection via the clusters before arriving at the MR; hence, the departure angles at the MT are related to the arrival angles at the MR. For multiple reflections, however, the departure angles are independent of the arrival angles; thus, the derivations and expressions of the model are also different. Vehicular channel models that consider multiple reflection clusters are described in our previous paper [38]. In the proposed model, we assume L clusters surround the MT and MR, in which we denote the ℓ-th ($\ell = 1, 2, \ldots, L$) cluster by $s^{(n_\ell)}$. Different clusters are modeled as resolvable paths with distinguishable propagation delays. For a single cluster, the cluster is modeled as a superposition of many unresolvable rays (subpaths). Here, we only depict the ℓ-th cluster. Other clusters can be depicted similarly but are omitted in this paper for brevity. Before proceeding, we specify the coordinate system and define the model parameters. At the initial instant, that is $t = 0$, the location of the MT (the black dot on the left) is assigned as the origin of the coordinate system, the line connecting the MT and the MR (the black dot on the right) is assigned as the x-axis, and the y-axis is chosen based on the right-hand rule. It is worth mentioning that $t = 0$ in [39] refers to a time interval during which the mobile terminals are stationary. In this study, however, the MT and MR are always in motion during the time interval of interest, and $t = 0$ only indicates a time instant from which we begin to observe the channel. Note that the coordinate system remains unchanged even though the MT, MR, and clusters move in the proposed model.

A. Complex Channel Impulse Response

In the proposed model, both the MT and MR are equipped with uniform linear arrays (ULAs), which consist of M_T and M_R omnidirectional antennas, respectively. The antenna inter-element spacings of the MT and MR arrays are denoted by δ_T and δ_R, respectively. The orientations of the ULA of the MT and MR with respect to the positive x-axis are denoted by ψ_T and ψ_R, respectively. Therefore, the complex channel impulse response (CIR) of the proposed MIMO channel model can be described by a matrix of size $M_R \times M_T$, that is, $\mathbf{H}(t, \tau) = [h_{pq}(t, \tau)]_{M_R \times M_T}$, where $h_{pq}(t, \tau)$ denotes the complex CIR between the p-th ($p = 1, 2, \ldots, M_T$) transmitting antenna and the q-th ($q = 1, 2, \ldots, M_R$) receiving antenna, which can be expressed as [40]

$$h_{pq}(t,\tau) = h_{pq}^{\mathrm{LoS}}(t)\delta\big(\tau - \tau^{\mathrm{LoS}}(t)\big) + \sum_{\ell=1}^{L} \chi_\ell h_{\ell,pq}(t)\delta\big(\tau - \tau_\ell(t)\big), \quad (1)$$

where χ_ℓ is the complex gain of path ℓ (cluster $s^{(n_\ell)}$). $\tau^{\mathrm{LoS}}(t) = D(t)/c$ is the time-varying propagation delay of the line-of-sight (LoS) component, where $D(t)$ designates the time-varying direct propagation path length between the centers of the MT and MR arrays, and $c = 3.0 \times 10^8$ m/s is the speed of light. $\tau_\ell(t)$ denotes the time-varying propagation delay of the ℓ-th non-LoS (NLoS) path, which can be expressed as $\tau_\ell(t) = \big(D_{T,\ell}(t) + D_{R,\ell}(t)\big)/c$, where $D_{T,\ell}(t)$ and $D_{R,\ell}(t)$ denote the time-varying propagation path lengths

from the centers of the MT and MR arrays to cluster $s^{(n_\ell)}$, respectively. It should be noted that for the NLoS components, the delays of different paths are distinct. Moreover, for each single path, the propagation delay can vary continuously over time owing to the motion of the MT, MR, and clusters. Therefore, the complex channel responses of the LoS and NLoS propagation links, denoted by $h_{pq}^{\mathrm{LoS}}(t)$ and $h_{\ell,pq}(t)$, respectively, can be expressed as

$$h_{pq}^{\mathrm{LoS}}(t) = \sqrt{\frac{\Omega}{\Omega+1}} e^{-j\frac{2\pi}{\lambda}D(t)} e^{j2\pi\int_0^t f_D^{\mathrm{LoS}}(t')dt'} \times e^{j\frac{2\pi}{\lambda}k_p\cos\left(\alpha_T^{\mathrm{LoS}}(t)-\psi_T\right)} e^{j\frac{2\pi}{\lambda}k_q\cos\left(\alpha_R^{\mathrm{LoS}}(t)-\psi_R\right)}, \tag{2}$$

$$h_{\ell,pq}(t) = \sqrt{\frac{1}{\Omega+1}}\sum_{n=1}^{N_\ell}\sqrt{\frac{1}{N_\ell}} e^{j\left(\varphi_0-\frac{2\pi}{\lambda}\left(D_{T,\ell,n}(t)+D_{R,\ell,n}(t)\right)\right)} \times e^{j\frac{2\pi}{\lambda}k_p\cos\left(\alpha_{T,\ell,n}(t)-\psi_T\right)} e^{j\frac{2\pi}{\lambda}k_q\cos\left(\alpha_{R,\ell,n}(t)-\psi_R\right)} \times e^{j2\pi\int_0^t f_{D,\ell,n}(t')dt'}, \tag{3}$$

where N_ℓ denotes the number of subpaths with unresolvable propagation delays for cluster $s^{(n_\ell)}$, Ω is the Rice factor, λ denotes the wavelength, $k_p = \frac{M_T-2p+1}{2}\delta_T$, $k_q = \frac{M_R-2q+1}{2}\delta_R$, and $D_{T,\ell,n}(t)$ and $D_{R,\ell,n}(t)$ denote the time-varying propagation path lengths of the ℓ-th NLoS component from the centers of the MT and MR arrays to the cluster $s^{(n_\ell)}$ via the n-th subpath, respectively. In addition, $\alpha_T^{\mathrm{LoS}}(t)$ and $\alpha_R^{\mathrm{LoS}}(t)$ denote the angle of departure (AoD) and angle of arrival (AoA) of the LoS component, whereas $\alpha_{T,\ell,n}(t)$ and $\alpha_{R,\ell,n}(t)$ denote the AoD and AoA of the waves from the MT and MR to cluster $s^{(n_\ell)}$ via the n-th subpath, respectively, both are time-varying. Moreover, $f_D^{\mathrm{LoS}}(t)$ and $f_{D,\ell,n}(t)$ denote the Doppler frequencies of the LoS component and that of the n-th ray in cluster $s^{(n_\ell)}$, respectively. Note that the time-varying properties of the Doppler frequencies are caused by the time-varying moving speeds and directions of the mobile transceivers and clusters. In this case, the phase shifts caused by the Doppler frequencies should be calculated by integrating $f_D^{\mathrm{LoS}}(t)$ and $f_{D,\ell,n}(t)$ with respect to time t instead of multiplying $f_D^{\mathrm{LoS}}(t)$ and $f_{D,\ell,n}(t)$ by t, as in the conventional models [31], [40], and [41]. It should be noted that for the NLoS components, the wave traveling distances from the centers of the MT and MR arrays to different scatterers in the same cluster are approximately equal. Hence, it is reasonable to use the cluster delay to model the propagation delay of the subpaths in the same cluster, that is, $\tau_\ell(t) \approx \tau_{\ell,1}(t) \cdots \approx \tau_{\ell,N_\ell}(t)$. Finally, φ_0 is a random phase angle that follows a uniform distribution in the interval from $-\pi$ to π, i.e., $\varphi_0 \sim \mathrm{U}[-\pi,\pi)$.

At the initial time instant $t = 0$, the propagation delay, propagation path length, AoD, and AoA of the LoS component are denoted by $\tau^{\mathrm{LoS}}(0)$, $D(0)$, $\alpha_T^{\mathrm{LoS}}(0)$, and $\alpha_R^{\mathrm{LoS}}(0)$, respectively. For the NLoS components, they are denoted by $\tau_\ell(0)$, $D_{T,\ell,n}(0)$, $D_{R,\ell,n}(0)$, $\alpha_{T,\ell,n}(0)$, and $\alpha_{R,\ell,n}(0)$, respectively. It is worth mentioning that $\tau^{\mathrm{LoS}}(0) = D(0)/c$, $\alpha_T^{\mathrm{LoS}}(0) = 0$, $\alpha_R^{\mathrm{LoS}}(0) = \pi$, and $\tau_\ell(0) = \left(D_{T,\ell}(0) + D_{R,\ell}(0)\right)/c$ at the initial instant. Then, by exploiting the geometrical relationship among the MT, MR, and clusters, we can obtain the propagation path lengths of the waves from the centers of the MT and MR arrays to cluster $s^{(n_\ell)}$ via the n-th subpath at the initial instant, which are denoted by $D_{T,\ell,n}(0)$ and $D_{R,\ell,n}(0)$, respectively, and expressed as

$$D_{R,\ell,n}(0) = \frac{\left(c\tau_\ell(0)\right)^2 - D^2(0)}{2c\tau_\ell(0) + 2D(0)\cos\alpha_{R,\ell,n}(0)}, \tag{4}$$

$$D_{T,\ell,n}(0) = \frac{(c\tau_\ell(0))^2 + D^2(0) + 2c\tau_\ell(0)D(0)\cos\alpha_{R,\ell,n}(0)}{2c\tau_\ell(0) + 2D(0)\cos\alpha_{R,\ell,n}(0)}, \tag{5}$$

and the corresponding AoD of the waves impinging on cluster $s^{(n_\ell)}$ via the n-th subpath in the representation of the AoA $\alpha_{R,\ell,n}(0)$ can be expressed in (6), as shown at the bottom of the next page.

Note that the initial distances $D(0)$, $D_{T,\ell}(0)$, and $D_{R,\ell}(0)$ as well as the received signal direction $\alpha_{R,\ell,n}(0)$ can be obtained by practical measurements or generated by some specific distributions. In the following section, we consider the non-stationary properties of the proposed V2X channel model introduced by the moving transceivers and clusters.

B. Motion of the MT, MR, and Clusters

Regarding the motion of the MT and MR, most of the existing V2X channel models used over-simplified mobility trajectories, that is, constant speed and direction or simple first-order linear functions, which limit the scope of the models and hence cannot be used to describe complicated scenarios such as S-shaped paths, crossroads, and time-varying traffic in realistic V2X communications. To address this limitation, we define the MT and MR in motion with time-varying accelerations, which means that the terminals in the proposed model can change their velocities and trajectories in a more general way, i.e., time-varying speed/angular accelerations, thus making the model more appropriate for describing realistic V2X communication scenarios. Nevertheless, by relaxing the motion model, i.e., setting some parameters as zeros, the proposed model can cover all the scenarios that the existing V2X channel models are available. To reduce the computational complexity of the model, we adopt linear functions to model the time-varying accelerations of the MT and MR. Specifically, the time-varying speed accelerations of the MT in the x and y directions can be expressed as $v_{T,x}^a(t) = v_{T,x}^a(0) + v_{T,x}^{a2}t$ and $v_{T,y}^a(t) = v_{T,y}^a(0) + v_{T,y}^{a2}t$, respectively, where $v_{T,x}^a(0)$ and $v_{T,y}^a(0)$ denote the initial speed accelerations of the MT in these two directions, and $v_{T,x}^{a2}$ and $v_{T,y}^{a2}$ are the gradients of $v_{T,x}^a(t)$ and $v_{T,y}^a(t)$, respectively. Then, the moving speeds of the MT in these two directions, denoted by $v_{T,x}(t)$ and $v_{T,y}(t)$, respectively, can be expressed as

$$v_{T,x}(t) = v_{T,x}(0) + \int_0^t v_{T,x}^a(t')dt', \tag{7}$$

$$v_{T,y}(t) = v_{T,y}(0) + \int_0^t v_{T,y}^a(t')dt', \tag{8}$$

where $v_{T,x}(0)$ and $v_{T,y}(0)$ are the initial speeds of the MT in the x and y directions, respectively. Similarly, at the

MR, the moving speeds are denoted by $v_{R,x}(t)$ and $v_{R,y}(t)$, respectively, and are expressed as

$$v_{R,x}(t) = v_{R,x}(0) + \int_0^t \left(v_{R,x}^a(0) + v_{R,x}^{a2}t'\right)dt', \quad (9)$$

$$v_{R,y}(t) = v_{R,y}(0) + \int_0^t \left(v_{R,y}^a(0) + v_{R,y}^{a2}t'\right)dt', \quad (10)$$

where $v_{R,x}(0)$ and $v_{R,y}(0)$ are the initial speeds of the MR in the x and y directions, respectively. Moreover, $v_{R,x}^a(0)$ and $v_{R,y}^a(0)$ denote the initial accelerations of the MR in the x and y directions, respectively, and $v_{R,x}^{a2}$ and $v_{R,y}^{a2}$ represent the gradients of the accelerations $v_{R,x}^a(t)$ and $v_{R,y}^a(t)$, respectively. According to Newton's second law of motion, the time-varying nature of the accelerations indicates that the force applied on the terminals has time-varying properties. Furthermore, the gradient v^{a2} implies that the force applied to the terminals increases or decreases over time, which generally accounts for the variation of the accelerations. As the values of the parameters in (7)-(10) can be arbitrarily chosen, the proposed multi-mobility model can describe different moving scenarios of the V2X channel, that is, M2M with constant velocity variations by imposing $v_{T,x}^{a2} = v_{T,y}^{a2} = v_{R,x}^{a2} = v_{R,y}^{a2} = 0$ and M2M with constant velocities by imposing $v_{T,x}^a(t) = v_{T,y}^a(t) = v_{R,x}^a(t) = v_{R,y}^a(t) = 0$, etc. Other moving scenarios of the proposed V2X channel model can be obtained by imposing appropriate values for the motion parameters. A detailed discussion is presented in Section IV.

Therefore, based on the mobility model presented in (7) and (8), the updated motion of the MT in the x and y directions at time t can be, respectively, expressed as

$$r_T^x(t) = \int_0^t v_{T,x}(t')dt' = v_{T,x}(0)t + \int_0^t \int_0^{t'} v_{T,x}^a(t'')dt''dt', \quad (11)$$

$$r_T^y(t) = \int_0^t v_{T,y}(t')dt' = v_{T,y}(0)t + \int_0^t \int_0^{t'} v_{T,y}^a(t'')dt''dt', \quad (12)$$

where $r_T^x(t)$ and $r_T^y(t)$ denote the moving displacements of the MT in the x and y directions, respectively. Then, the time-varying location of the MT can be denoted by the vector $\mathbf{r}_T(t) = [r_T^x(t), r_T^y(t)]^T$, where the superscript $[\cdot]^T$ is the transpose operator. Similarly, based on the mobility model presented in (9) and (10), the moving displacements of the MR in the x and y directions, denoted by $r_R^x(t)$ and $r_R^y(t)$, respectively, can be expressed as

$$r_R^x(t) = \int_0^t v_{R,x}(t')dt' = v_{R,x}(0)t + \int_0^t \int_0^{t'} v_{R,x}^a(t'')dt''dt', \quad (13)$$

$$r_R^y(t) = \int_0^t v_{R,y}(t')dt' = v_{R,y}(0)t + \int_0^t \int_0^{t'} v_{R,y}^a(t'')dt''dt'. \quad (14)$$

As demonstrated in [42], the movements of the clusters can also result in non-stationarity of the V2X channels. It should be noted that when modeling the motion of the clusters, most of the existing literature applied an over-simplified mobility model, that is, a model with a constant velocity and direction [36], [40], and [43]. However, the motion of the clusters is generally complicated and difficult to determine in practice. For example, let us consider a UAV hovering at a low altitude as a cluster in the proposed V2X communication scenario. The cluster can experience random perturbation owing to the effects of the environment, such as wind. Consequently, it is generally difficult to define and acquire the actual moving speeds and directions of the clusters. Thus, the existing models will, in principle, lead to inaccurate description of the channel statistical properties. A few studies have introduced random mobility models in non-stationary channel modeling [44], [45]. In contrast, random walk, is considered an effective model for characterizing the random position of the mobile objects induced by unpredictable factors and can achieve a reasonable tradeoff between accuracy and analytical tractability [46]. Under these considerations, we model the motion of the clusters by random walk and the time-varying positions of the clusters by random variables to investigate the impact of the randomness of cluster motion on channel statistic properties. It should be noted that when modeling the motion of the clusters, the scatterers in the same cluster are generally assumed to have the same kinematic properties, which means that the scatterers in the same cluster can be regarded as a unit when they are in motion. The movements of the clusters in the proposed multi-mobility V2X channel model are decomposed into two independent random walks with the same kinematic properties along the x-axis and y-axis. Let $\Delta x_\ell(t)$ and $\Delta y_\ell(t)$ be the moving displacements of the cluster $s^{(n_\ell)}$ in the x and y directions after a time interval t, respectively. Then, the displacements $\Delta x_\ell(t)$ and $\Delta y_\ell(t)$ can be modeled as two zero-mean Gaussian random processes with the same variance, and the corresponding probability density function (PDF) of the moving displacements for the cluster $s^{(n_\ell)}$ is given by

$$f_i(i,t) = \frac{1}{\sqrt{2\pi\sigma_i^2(t)}} e^{-i^2/2\sigma_i^2(t)}, \quad (15)$$

for $i \in \{\Delta x_\ell, \Delta y_\ell\}$, where $\sigma_{\Delta x_\ell}^2(t) = \sigma_{\Delta y_\ell}^2(t) = \omega_\ell t$ denotes the time-varying variance of the displacements $\Delta x_\ell(t)$ and $\Delta y_\ell(t)$, and ω_ℓ is a constant value. Figure 2 presents four possible trajectory variations of cluster $s^{(n_\ell)}$ following a random walk process.

C. Updated Model Parameters

As shown in Fig. 1, after a time interval t, the MT and MR move from the locations of the black dots to the locations of the red dots. Generally, the clusters in the channel can exist over a certain time period, which means that the number of

$$\alpha_{T,\ell,n}(0) = \arccos\left\{\frac{2c\tau_\ell(0)D(0) + D^2(0)\cos\alpha_{R,\ell,n}(0) + \left(c\tau_\ell(0)\right)^2\cos\alpha_{R,\ell,n}(0)}{\left(c\tau_\ell(0)\right)^2 + 2c\tau_\ell(0)D(0)\cos\alpha_{R,\ell,n}(0) + D^2(0)}\right\}. \quad (6)$$

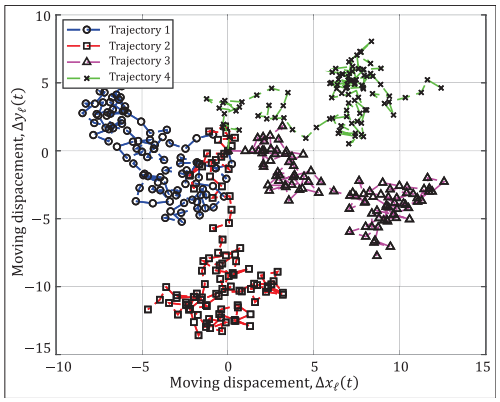

Fig. 2. Illustration of the possible trajectories of the random walking clusters.

clusters does not change frequently and can be regarded as constant during this period. Therefore, only the time-varying parameters are updated as follows. To acquire the time-varying model parameters, we introduce the vector representation in Cartesian coordinates. The real-time direct distance vector from the center of the MT array to that of the MR array can be expressed as

$$\mathbf{d}(t) = \begin{bmatrix} D(0) - r_T^x(t) + r_R^x(t) \\ r_R^y(t) - r_T^y(t) \end{bmatrix}. \tag{16}$$

In this way, the time-varying propagation delay of the LoS propagation link can be derived as $\tau^{\mathrm{LoS}}(t) = \|\mathbf{d}(t)\|/c$, where $\|\cdot\|$ denotes the ℓ_2-norm of vector.

It is worth mentioning that the motion of the clusters follows a random walk process and the moving displacement of the clusters can be decomposed into two independent zero-mean Gaussian random processes with the same time-varying variance. Moreover, the time interval of interest is generally a short duration and the displacements of the clusters are short with respect to the propagation path lengths. As a result, the perturbations of the propagation path lengths and angular parameters induced by the random movements of the clusters can be neglected, which means that the location variations of the clusters are negligiable as compared to those of the MT and MR. Therefore, the real-time distance vector from the center of the MT array to cluster $s^{(n_\ell)}$ via the n-th subpath can be expressed as

$$\mathbf{d}_{T,\ell,n}(t) = \begin{bmatrix} D_{T,\ell,n}(0)\cos\alpha_{T,\ell,n}(0) - r_T^x(t) \\ D_{T,\ell,n}(0)\sin\alpha_{T,\ell,n}(0) - r_T^y(t) \end{bmatrix}. \tag{17}$$

Then, the averaged real-time propagation path length from the center of the MT array to cluster $s^{(n_\ell)}$ can be calculated by

$$D_{T,\ell}(t) = \frac{1}{N_\ell}\sum_{n=1}^{N_\ell} \|\mathbf{d}_{T,\ell,n}(t)\|. \tag{18}$$

Similarly, the real-time distance vector from the center of the MR array to cluster $s^{(n_\ell)}$ via the n-th subpath can be expressed as

$$\mathbf{d}_{R,\ell,n}(t) = \begin{bmatrix} D_{R,\ell,n}(0)\cos\alpha_{R,\ell,n}(0) - r_R^x(t) \\ D_{R,\ell,n}(0)\sin\alpha_{R,\ell,n}(0) - r_R^y(t) \end{bmatrix}. \tag{19}$$

Meanwhile, the corresponding averaged real-time propagation path length from the center of the MR array to cluster $s^{(n_\ell)}$ can be calculated by

$$D_{R,\ell}(t) = \frac{1}{N_\ell}\sum_{n=1}^{N_\ell} \|\mathbf{d}_{R,\ell,n}(t)\|. \tag{20}$$

Furthermore, the time-varying AoD and AoA for the LoS link can be derived as

$$\alpha_T^{\mathrm{LoS}}(t) = \arcsin \frac{r_R^y(t) - r_T^y(t)}{\sqrt{\left(D(0) - r_T^x(t) + r_R^x(t)\right)^2 + \left(r_R^y(t) - r_T^y(t)\right)^2}}, \tag{21}$$

$$\alpha_R^{\mathrm{LoS}}(t) = \begin{cases} \alpha_T^{\mathrm{LoS}}(t) - \pi, & \text{if } \alpha_T^{\mathrm{LoS}}(t) > 0 \\ \alpha_T^{\mathrm{LoS}}(t) + \pi, & \text{if } \alpha_T^{\mathrm{LoS}}(t) \le 0 \end{cases}. \tag{22}$$

Finally, the time-varying AoD $\alpha_{T,\ell,n}(t)$ and AoA $\alpha_{R,\ell,n}(t)$ can be expressed as (23) and (24), as shown at the bottom of the next page.

D. Doppler Frequency Analysis

Owing to the velocity variations of the MT and MR as well as the random motion of the clusters, the Doppler frequencies $f_D^{\mathrm{LoS}}(t)$ and $f_{D,\ell,n}(t)$ can vary over time. Consequently, the Doppler phase shifts, that is, $\varphi_D^{\mathrm{LoS}}(t)$ and $\varphi_{D,\ell,n}(t)$, should be carefully calculated instead of simply multiplying the Doppler frequencies by time.

For the LoS component, the time-varying nature of $f_D^{\mathrm{LoS}}(t)$ is caused by the motion of MT and MR, and not by the motion of clusters. Therefore, $f_D^{\mathrm{LoS}}(t)$ can be expressed as (25), as shown at the bottom of the next page. Then, by substituting (21) and (22) into (25), we can further derive the Doppler phase shift of the LoS component by $\varphi_D^{\mathrm{LoS}}(t) = 2\pi\int_0^t f_D^{\mathrm{LoS}}(t')dt'$.

For the NLoS components, the Doppler frequency $f_{D,\ell,n}(t)$ is related to the velocity variations of the MT and MR as well as the random motion of the clusters. Furthermore, deriving the instantaneous moving speeds of the clusters is challenging. As a result, the expansion form of $f_{D,\ell,n}(t)$ is complicated, and the integration process to obtain the Doppler phase shift $\varphi_{D,\ell,n}(t)$ has high computational complexity. To address this issue, the time interval $[0, t)$ is divided into Γ slots with the same slot duration, that is, $\Gamma = t/\Delta t$. During each slot, the time-varying Doppler frequency can be approximated by a constant value as the slot duration Δt is sufficiently small. To some extent, the channel stationary time intervals can be used as a metric of slot duration. For example, the channel stationary intervals are approximately 39 ms at a speed of 30 m/s and 292 ms at a speed 5 m/s [41]. Then, the slot durations can be set as 10 ms and 70 ms, respectively, which are a quarter of the stationary intervals. In this case, the integrated phase $\varphi_{D,\ell,n}(t)$ during the interval from $t' = 0$ to t can be approximated as

$$\varphi_{D,\ell,n}(t) = 2\pi\int_0^t f_{D,\ell,n}(t')dt' \approx 2\pi\sum_{m=1}^{\Gamma} f_{D,\ell,n}(m\Delta t)\Delta t, \tag{26}$$

where $f_{D,\ell,n}(m\Delta t) = f^T_{D,\ell,n}(m\Delta t) + f^R_{D,\ell,n}(m\Delta t)$ denotes the Doppler frequency during the m-th ($m = 1, 2, \ldots, \Gamma$) slot, which is approximated by the value at the instant $\frac{m}{\Gamma}t$. Moreover, $f^T_{D,\ell,n}(m\Delta t)$ and $f^R_{D,\ell,n}(m\Delta t)$ denote the Doppler frequencies observed at the cluster and MR during the m-th slot, respectively. As shown in (15), the moving displacements of cluster $s^{(n_\ell)}$ in the x and y directions during the time interval from the instant of $(m-1)\Delta t$ to the instant of $m\Delta t$ are denoted by $\Delta x_{\ell,m}(\Delta t)$ and $\Delta y_{\ell,m}(\Delta t)$, respectively, and both of them are zero-mean Gaussian random variables with variance $\omega_\ell \Delta t$. It is assumed that the slot duration Δt is sufficiently small, and hence the time-varying moving velocity of the cluster in the m-th slot can be approximated by the average moving speeds in the x and y directions, and they can be calculated by $\frac{\Delta x_{\ell,m}(\Delta t)}{\Delta t}$ and $\frac{\Delta y_{\ell,m}(\Delta t)}{\Delta t}$, respectively. Therefore, the Doppler frequency observed at the cluster during the m-th slot can be expressed as

$$f^T_{D,\ell,n}(m\Delta t) = \frac{1}{\lambda}\left[\cos\alpha_{T,\ell,n}(m\Delta t), \sin\alpha_{T,\ell,n}(m\Delta t)\right] \times \begin{bmatrix} v_{T,x}(m\Delta t) - \frac{\Delta x_{\ell,m}(\Delta t)}{\Delta t} \\ v_{T,y}(m\Delta t) - \frac{\Delta y_{\ell,m}(\Delta t)}{\Delta t} \end{bmatrix}, \quad (27)$$

where $v_{T,x}(m\Delta t)$ and $v_{T,y}(m\Delta t)$ denote the moving speeds of the MT in the x and y directions at the instant $\frac{m}{\Gamma}t$, respectively, which can be derived from (7) and (8), and $\alpha_{T,\ell,n}(m\Delta t)$ denotes the AoD at the instant $\frac{m}{\Gamma}t$, which can be derived from (23).

Similarly, the Doppler frequency observed at the MR during the m-th slot can be expressed as

$$f^R_{D,\ell,n}(m\Delta t) = \frac{1}{\lambda}\left[\cos\alpha_{R,\ell,n}(m\Delta t), \sin\alpha_{R,\ell,n}(m\Delta t)\right] \times \begin{bmatrix} v_{R,x}(m\Delta t) - \frac{\Delta x_{\ell,m}(\Delta t)}{\Delta t} \\ v_{R,y}(m\Delta t) - \frac{\Delta y_{\ell,m}(\Delta t)}{\Delta t} \end{bmatrix}, \quad (28)$$

where $v_{R,x}(m\Delta t)$ and $v_{R,y}(m\Delta t)$ denote the moving speeds of the MR in the x and y directions at the instant $\frac{m}{\Gamma}t$, respectively, which can be derived from (9) and (10), and $\alpha_{R,\ell,n}(m\Delta t)$ denotes the AoA at the instant $\frac{m}{\Gamma}t$, which can be derived from (24).

By substituting (27) and (28) into (26), the Doppler phase shift $\varphi_{D,\ell,n}(t)$ caused by motion of the MT, MR, and cluster $s^{(n_\ell)}$ can be approximated by

$$\begin{aligned}\varphi_{D,\ell,n}(t) \approx \frac{2\pi}{\lambda}\sum_{m=1}^{\Gamma}\Big[&v_{T,x}(m\Delta t)\cos\alpha_{T,\ell,n}(m\Delta t) \\ &+ v_{R,x}(m\Delta t)\cos\alpha_{R,\ell,n}(m\Delta t) \\ &+ v_{T,y}(m\Delta t)\sin\alpha_{T,\ell,n}(m\Delta t) \\ &+ v_{R,y}(m\Delta t)\sin\alpha_{R,\ell,n}(m\Delta t)\Big]\Delta t \\ -\frac{2\pi}{\lambda}\sum_{m=1}^{\Gamma}\Big[&\Delta x_{\ell,m}(\Delta t)\big(\cos\alpha_{T,\ell,n}(m\Delta t) \\ &+ \cos\alpha_{R,\ell,n}(m\Delta t)\big) \\ &+ \Delta y_{\ell,m}(\Delta t)\big(\sin\alpha_{T,\ell,n}(m\Delta t) \\ &+ \sin\alpha_{R,\ell,n}(m\Delta t)\big)\Big]. \end{aligned} \quad (29)$$

Because of the random properties of the displacements $\Delta x_{\ell,m}(\Delta t)$ and $\Delta y_{\ell,m}(\Delta t)$, the second summation term in (29) is a random process, while the first summation term in (29) is a deterministic process. It has been assumed that the displacements $\Delta x_{\ell,m}(\Delta t)$ and $\Delta y_{\ell,m}(\Delta t)$ are two independent zero-mean Gaussian random variables with the same variances $\omega_\ell \Delta t$. In addition, the displacements of the clusters in different slots are also independent of each other. Therefore, the second summation term in (29) can be modeled as the sum of 2Γ independent Gaussian random variables. Consequently, the Doppler phase shift $\varphi_{D,\ell,n}(t)$ is also a Gaussian random process. As the slot duration is sufficiently small, the time-varying mean value of the phase $\varphi_{D,\ell,n}(t)$,

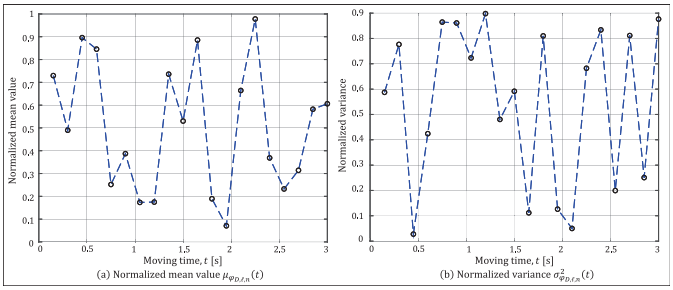

Fig. 3. Time-varying properties of $\varphi_{D,\ell,n}(t)$, (a) normalized mean value $\mu_{\varphi_{D,\ell,n}}(t)$, (b) normalized variance $\sigma^2_{\varphi_{D,\ell,n}}(t)$.

$$\alpha_{T,\ell,n}(t) = \arccos\frac{D_{T,\ell,n}(0)\cos\alpha_{T,\ell,n}(0) - r^x_T(t)}{\sqrt{\left(D_{T,\ell,n}(0)\cos\alpha_{T,\ell,n}(0) - r^x_T(t)\right)^2 + \left(D_{T,\ell,n}(0)\sin\alpha_{T,\ell,n}(0) - r^y_T(t)\right)^2}}, \quad (23)$$

$$\alpha_{R,\ell,n}(t) = \arccos\frac{D_{R,\ell,n}(0)\cos\alpha_{R,\ell,n}(0) - r^x_R(t)}{\sqrt{\left(D_{R,\ell,n}(0)\cos\alpha_{R,\ell,n}(0) - r^x_R(t)\right)^2 + \left(D_{R,\ell,n}(0)\sin\alpha_{R,\ell,n}(0) - r^y_R(t)\right)^2}}. \quad (24)$$

$$\begin{aligned} f^{\text{LoS}}_D(t) &= \frac{1}{\lambda}\left[\cos\alpha^{\text{LoS}}_T(t), \sin\alpha^{\text{LoS}}_T(t)\right]\begin{bmatrix} v_{T,x}(t) \\ v_{T,y}(t)\end{bmatrix} + \frac{1}{\lambda}\left[\cos\alpha^{\text{LoS}}_R(t), \sin\alpha^{\text{LoS}}_R(t)\right]\begin{bmatrix} v_{R,x}(t) \\ v_{R,y}(t)\end{bmatrix} \\ &= \frac{1}{\lambda}\big(v_{T,x}(t)\cos\alpha^{\text{LoS}}_T(t) + v_{T,y}(t)\sin\alpha^{\text{LoS}}_T(t) + v_{R,x}(t)\cos\alpha^{\text{LoS}}_R(t) + v_{R,y}(t)\sin\alpha^{\text{LoS}}_R(t)\big). \end{aligned} \quad (25)$$

denoted by $\mu_{\varphi_{D,\ell,n}}(t) = \mathbb{E}\{\varphi_{D,\ell,n}(t)\}$, can be expressed as

$$\mu_{\varphi_{D,\ell,n}}(t) = \frac{2\pi}{\lambda}\int_0^t \Big[v_{T,x}(t')\cos\alpha_{T,\ell,n}(t') + v_{R,x}(t')\cos\alpha_{R,\ell,n}(t') + v_{T,y}(t')\sin\alpha_{T,\ell,n}(t') + v_{R,y}(t')\sin\alpha_{R,\ell,n}(t')\Big]dt', \tag{30}$$

and the corresponding variance, denoted by $\sigma^2_{\varphi_{D,\ell,n}}(t) = Var\{\varphi_{D,\ell,n}(t)\}$, can be expressed as

$$\sigma^2_{\varphi_{D,\ell,n}}(t) = \frac{8\pi^2\omega_\ell}{\lambda^2}\Big(t + \int_0^t \big(\cos\alpha_{T,\ell,n}(t')\cos\alpha_{R,\ell,n}(t') + \sin\alpha_{T,\ell,n}(t')\sin\alpha_{R,\ell,n}(t')\big)dt'\Big). \tag{31}$$

Therefore, the PDF of the time-varying random phase $\varphi_{D,\ell,n}(t)$, caused by the movements of the MT, MR, and the clusters, can be expressed as

$$f_{\varphi_{D,\ell,n}(t)}(\varphi_{D,\ell,n},t) = \frac{\exp\left\{-\frac{\left(\varphi_{D,\ell,n}-\mu_{\varphi_{D,\ell,n}}(t)\right)^2}{2\sigma^2_{\varphi_{D,\ell,n}}(t)}\right\}}{\sqrt{2\pi\sigma^2_{\varphi_{D,\ell,n}}(t)}}. \tag{32}$$

Figure 3(a) shows the time-varying property of the normalized mean value $\mu_{\varphi_{D,\ell,n}}(t)$ in (30) and Fig. 3(b) shows that of the normalized variance $\sigma^2_{\varphi_{D,\ell,n}}(t)$ in (31). They show that the mean value and variance of the Gaussian distributed Doppler phase shift $\varphi_{D,\ell,n}(t)$ can vary rapidly over moving time t, owing to the velocity variations of the MT and MR as well as the random motion of the clusters. Note that the approximated closed-form expressions of $\mu_{\varphi_{D,\ell,n}}(t)$ and $\sigma^2_{\varphi_{D,\ell,n}}(t)$ are given in Appendix A.

III. Statistical Properties of the Proposed Channel Model

In this section, we describe the channel characteristics of the proposed channel model, including the local spatial-temporal (ST) cross-correlation function (CCF), the temporal auto-correlation function (ACF), the frequency correlation function (FCF), and the power delay profile (PDP).

A. Time-Varying Local ST CCF

As shown in [26], [47], the local correlation properties of a MIMO V2V channel are completely determined by the correlation properties between $h_{\ell,pq}(t)$ and $h_{\ell,p'q'}(t+\tau')$ in each tap. Furthermore, it is generally assumed that there is no correlation between different links; meanwhile, the local ST correlation properties of the non-stationary MIMO channel are jointly dependent on time t and the relative antenna element spacing at the MT and MR arrays. Therefore, the normalized local ST CCF between $h_{\ell,pq}(t)$ and $h_{\ell,p'q'}(t+\tau')$ can be defined as [41]

$$\rho_{(p,q),(p',q'),\ell}(t,\Delta p,\Delta q,\tau') = \frac{\mathbb{E}\big[h_{\ell,pq}(t)h^*_{\ell,p'q'}(t+\tau')\big]}{\sqrt{\mathbb{E}\big[|h_{\ell,pq}(t)|^2\big]\mathbb{E}\big[|h_{\ell,p'q'}(t+\tau')|^2\big]}}, \tag{33}$$

where τ' denotes the time difference, $\mathbb{E}[\cdot]$ is the statistical average, the superscript $[\cdot]^*$ is the complex conjugation operator, and $\Delta p = |p'-p|\delta_T/\lambda$ and $\Delta q = |q'-q|\delta_R/\lambda$ denote the normalized antenna spacings of the MT and MR arrays, respectively, where p, p', q, and q' are the antenna indexes. In addition, $h_{\ell,pq}(t)$ and $h_{\ell,p'q'}(t+\tau')$ denote the complex channel coefficients of the $(p \to q)$-th and $(p' \to q')$-th transmit-receive antenna pair, respectively.

It is worth mentioning that the LoS component $h^{\text{LoS}}_{pq}(t)$ and NLoS components $h_{\ell,pq}(t)$ of the proposed model are assumed to be independent of each other; hence, there is no correlation between $h^{\text{LoS}}_{pq}(t)$ and $h_{\ell,pq}(t)$ [13]. Then, by substituting (1) into (33), we get the local ST CCF as

$$\rho_{(p,q),(p',q'),\ell}(t,\Delta p,\Delta q,\tau') = \rho^{\text{LoS}}_{(p,q),(p',q')}(t,\Delta p,\Delta q,\tau') + \rho^{\text{NLoS}}_{(p,q),(p',q'),\ell}(t,\Delta p,\Delta q,\tau'), \tag{34}$$

where $\rho^{\text{LoS}}_{(p,q),(p',q')}(t,\Delta p,\Delta q,\tau')$ and $\rho^{\text{NLoS}}_{(p,q),(p',q'),\ell}(t,\Delta p,\Delta q,\tau')$ are the local ST CCFs of the LoS and NLoS components, respectively, and are expressed as

$$\begin{aligned}\rho^{\text{LoS}}_{(p,q),(p',q')}(t,\Delta p,\Delta q,\tau') &= e^{j\frac{2\pi}{\lambda}\left(D(t+\tau')-D(t)\right)} \\ &\times e^{j\frac{2\pi}{\lambda}\left(k_p\cos(\alpha^{\text{LoS}}_T(t)-\psi_T)-k_{p'}\cos(\alpha^{\text{LoS}}_T(t+\tau')-\psi_T)\right)} \\ &\times e^{j\frac{2\pi}{\lambda}\left(k_q\cos(\alpha^{\text{LoS}}_R(t)-\psi_R)-k_{q'}\cos(\alpha^{\text{LoS}}_R(t+\tau')-\psi_R)\right)} \\ &\times e^{j2\pi\left(\varphi^{\text{LoS}}_D(t)-\varphi^{\text{LoS}}_D(t+\tau')\right)},\end{aligned} \tag{35}$$

$$\begin{aligned}\rho^{\text{NLoS}}_{(p,q),(p',q'),\ell}(t,\Delta p,\Delta q,\tau') &= \frac{1}{N_\ell}\sum_{\ell=1}^{N_\ell}\mathbb{E}\{ \\ &\times e^{j\frac{2\pi}{\lambda}\left(D_{T,\ell,n}(t+\tau')-D_{T,\ell,n}(t)+D_{R,\ell,n}(t+\tau')-D_{R,\ell,n}(t)\right)} \\ &\times e^{j\frac{2\pi}{\lambda}\left(k_p\cos(\alpha_{T,\ell,n}(t)-\psi_T)-k_{p'}\cos(\alpha_{T,\ell,n}(t+\tau')-\psi_T)\right)} \\ &\times e^{j\frac{2\pi}{\lambda}\left(k_q\cos(\alpha_{R,\ell,n}(t)-\psi_R)-k_{q'}\cos(\alpha_{R,\ell,n}(t+\tau')-\psi_R)\right)} \\ &\times e^{j\left(\varphi_{D,\ell,n}(t)-\varphi_{D,\ell,n}(t+\tau')\right)}\}.\end{aligned} \tag{36}$$

By setting the time difference $\tau' = 0$ in (35), we can obtain the following spatial CCF for the LoS component:

$$\rho^{\text{LoS}}_{(p,q),(p',q')}(t,\Delta p,\Delta q) = e^{j2\pi\Delta p\cos\left(\alpha^{\text{LoS}}_T(t)-\psi_T\right)}e^{j2\pi\Delta q\cos\left(\alpha^{\text{LoS}}_R(t)-\psi_R\right)}. \tag{37}$$

For the NLoS components, the corresponding spatial CCF can be derived by imposing $\tau' = 0$ in (36), which yields

$$\rho_{(p,q),(p',q'),\ell}(t,\Delta p,\Delta q) = \int_{-\pi}^{\pi} e^{j2\pi\Delta p\cos\left(\alpha_{T,\ell}(t)-\psi_T\right)} \times e^{j2\pi\Delta q\cos\left(\alpha_{R,\ell}(t)-\psi_R\right)}f(\alpha_{R,\ell})d\alpha_{R,\ell}, \tag{38}$$

where $f(\alpha_{R,\ell})$ denotes the PDF of the received signal direction $\alpha_{R,\ell}$ of cluster $s^{(n_\ell)}$. In general, the AoA and AoD of the waves are dependent on each other in the proposed single-bounced channel model, and this relationship can be seen in (6). It is worth mentioning that in the cluster-based model, one cluster corresponds to one path; hence, the values of the signal directions are limited to a certain range. Here, we adopt the truncated Gaussian PDF to characterize the angular distribution. In this case, the PDF for the waves with the direction of α, whereby α varies in the interval from α_{low} to α_{up}, that is, $\alpha \in [\alpha_{low}, \alpha_{up}]$, can be expressed as

$$f(\alpha, \mu_\alpha, \sigma_\alpha, \alpha_{low}, \alpha_{up}) = \frac{\frac{1}{\sigma_\alpha}\phi\left(\frac{\alpha-\mu_\alpha}{\sigma_\alpha}\right)}{\Phi\left(\frac{\alpha_{up}-\mu_\alpha}{\sigma_\alpha}\right) - \Phi\left(\frac{\alpha_{low}-\mu_\alpha}{\sigma_\alpha}\right)}, \quad (39)$$

where μ_α and σ_α denote the mean value and angle spread of the signal direction α, respectively, and α_{low} and α_{up} denote the lower and upper bounds of the truncated Gaussian distributed signal direction α, respectively. Moreover, $\phi(\epsilon)$ is the PDF of the standard normally distributed random variable ϵ, which can be expressed as $\phi(\epsilon) = \frac{1}{2\pi} exp\{-\frac{\epsilon^2}{2}\}$, whereas $\Phi(\epsilon) = \int_{-\infty}^{\epsilon} \phi(\epsilon')d\epsilon' = \frac{1}{2}\left(1 + erf(\frac{\epsilon}{\sqrt{2}})\right)$ denotes the cumulative distribution function (CDF) of the standard normally distributed random variable ϵ, and $erf(\cdot)$ is the Gaussian error function.

Furthermore, by imposing $\Delta p = 0$ in (38), which means that the two links share the same transmit antenna, we can further obtain the spatial CCF observed at the MR as

$$\rho_{(p,q),(p',q'),\ell}(t, \Delta q) = \int_{\alpha_{R,\ell}^{low}}^{\alpha_{R,\ell}^{up}} e^{j2\pi\Delta q \cos\left(\alpha_{R,\ell}(t)-\psi_R\right)} f(\alpha_{R,\ell}) d\alpha_{R,\ell}, \quad (40)$$

where $f(\alpha_{R,\ell})$ denotes the marginal PDF of AoA for the cluster $s^{(n_\ell)}$, which is defined by (39) and can be obtained by replacing the parameters $(\alpha, \mu_\alpha, \sigma_\alpha, \alpha_{low}, \alpha_{up})$ with $(\alpha_{R,\ell}, \mu_{\alpha_{R,\ell}}, \sigma_{\alpha_{R,\ell}}, \alpha_{R,\ell}^{low}, \alpha_{R,\ell}^{up})$ for the initial AoA distribution. Similarly, by setting $\Delta q = 0$ in (38), which means that the two links share the same receive antenna, the spatial CCF observed at the MT can be obtained.

B. Time-Varying Temporal ACF

The temporal ACF of the proposed channel model can be obtained from the local ST CCF $\rho_{(p,q),(p',q'),\ell}(t, \Delta p, \Delta q, \tau')$ in (33) by setting $\Delta p = 0$ and $\Delta q = 0$, that is, $p = p'$ and $q = q'$, which can be expressed as [41]

$$\rho_\ell(t, \tau') = \rho^{\text{LoS}}(t, \tau') + \rho_\ell^{\text{NLoS}}(t, \tau'), \quad (41)$$

where $\rho^{\text{LoS}}(t, \tau')$ and $\rho_\ell^{\text{NLoS}}(t, \tau')$ denote the temporal ACF of the LoS and NLoS components, respectively, which are expressed as

$$\rho^{\text{LoS}}(t, \tau') = e^{-j\frac{2\pi}{\lambda}\left(D(t+\tau')-D(t)\right)} e^{j\left(\varphi_D^{\text{LoS}}(t)-\varphi_D^{\text{LoS}}(t+\tau')\right)}, \quad (42)$$

$$\rho_\ell^{\text{NLoS}}(t, \tau') = \frac{1}{N_\ell}\sum_{n=1}^{N_\ell} \mathbb{E}\Big\{ e^{j\left(\varphi_{D,\ell,n}(t)-\varphi_{D,\ell,n}(t+\tau')\right)} \times e^{j\frac{2\pi}{\lambda}\left(D_{T,\ell,n}(t+\tau')-D_{T,\ell,n}(t)+D_{R,\ell,n}(t+\tau')-D_{R,\ell,n}(t)\right)} \Big\}. \quad (43)$$

It can be seen from (41)-(43) that the temporal ACF $\rho_\ell(t, \tau')$ of the proposed channel model depends on time t, which means the channel is non-stationary. Thus, the WSS assumption that the temporal ACF only depends on the time difference τ' is no longer valid. Therefore, the proposed multi-mobility V2X channel model can characterize the non-stationary properties of mobile channels in B5G and 6G V2X communication environments.

C. Time-Varying FCF and PDP

The time-varying transfer function of the proposed channel model is defined as the Fourier transform of the complex CIR $h_{pq}(t, \tau)$ with respect to the propagation delay τ, which can be expressed as [48]

$$H_{pq}(t, f) = h_{pq}^{\text{LoS}}(t) e^{-j2\pi f \tau^{\text{LoS}}(t)} + \sum_{\ell=1}^{L} \chi_\ell(t) h_{\ell,pq}(t) e^{-j2\pi f \tau_\ell(t)}. \quad (44)$$

Based on (44), the normalized FCF of the proposed channel model is defined as [13]

$$\rho_{H_{pq}}(t, \Delta f) = \frac{\mathbb{E}\left[H_{pq}(t, f) H_{pq}^*(t, f+\Delta f)\right]}{\sqrt{\mathbb{E}\left[|H_{pq}(t, f)|^2\right]\mathbb{E}\left[|H_{pq}(t, f+\Delta f)|^2\right]}}, \quad (45)$$

where Δf denotes frequency separation. With the uncorrelated scattering (US) assumption [47], the substitution of (2), (3), and (44) into (45) can result in the following FCF:

$$\rho_{H_{pq}}(t, \Delta f) = \frac{\Omega}{\Omega+1} e^{j2\pi\Delta f \tau^{\text{LoS}}(t)} + \frac{1}{\Omega+1}\sum_{\ell=1}^{L} \chi_\ell^2 e^{j2\pi\Delta f \tau_\ell(t)}. \quad (46)$$

Then, by applying the inverse Fourier transform to the FCF $\rho_{H_{pq}}(t, \Delta f)$ with respect to frequency separation Δf, we can further derive the PDP of the proposed channel model as [26]

$$S_{H_{pq}}(t, \tau) = \frac{\Omega}{\Omega+1}\delta\left(\tau - \tau^{\text{LoS}}(t)\right) + \frac{1}{\Omega+1}\sum_{\ell=1}^{L} \chi_\ell^2 \delta\left(\tau - \tau_\ell(t)\right). \quad (47)$$

From (46) and (47), we observe that the FCF and PDP of the proposed channel model are dependent on time t, which conforms to the non-stationarity of the proposed model, and they can be determined by four parameters, that is, the Rice factor Ω, cluster number L, path gains χ_ℓ, and delays τ. Alternatively, by setting the LoS component $h_{pq}^{\text{LoS}}(t)$ in (1) as zero and ignoring the corresponding derivations and analysis for the LoS component, that is, CIR in (2), distance and angles in (16), (21), and (22), Doppler frequency in (25), and channel statistical properties in (35), (37), (42), (44), (46), and (47), the proposed model can be used to model the scenario with the LoS path obstructed.

IV. Results and Discussions

In this section, we investigate the impact of the velocity variations of the mobile terminals as well as the random walk of the clusters on the channel statistical properties of the proposed non-stationary multi-mobility V2X channel model.

A. Simulation Setup

The proposed V2X channel model is operated at a carrier frequency of $f_c = 5.9$ GHz. The parameters used in the simulations are listed here or specified otherwise: $M_T = M_R = 4$, $\delta_T = \delta_R = \lambda/2$, $\psi_T = \pi/4$, $\psi_R = \pi/3$, $D(0) = 120$ m, $D_{T,\ell}(0) = D_{R,\ell}(0) = 120$ m, $\mu_{\alpha_{R,\ell}} = 2.095$ rad, $\sigma_{\alpha_{R,\ell}} = 0.524$ rad, $\alpha_{R,\ell}^{low} = 1.571$ rad, and $\alpha_{R,\ell}^{up} = 2.619$ rad. For the random walk of the clusters, we assume that $\omega_\ell = 0.01$. For the velocity variations of the mobile terminals, the motion parameters of the MT and MR are specified under specific V2X communication scenarios. By setting different values to the motion parameters of the MT and MR, we can describe different V2X communication scenarios based on the proposed V2X channel model.

Case I: Velocity variations with time-varying accelerations The MT and MR both move with time-varying accelerations; hence, the mobile terminals can experience accelerations and decelerations, which makes the model more applicable to general and realistic V2X scenarios.

Case II: Velocity variations with constant accelerations The terminals experience velocity variations only in one direction, which means the speeds of the MT and MR either increase or decrease during the time period of interest [36]. This can be obtained by setting the accelerations as time-invariant, that is, $v_{T,x}^a(t) = v_{T,x}^a, v_{T,y}^a(t) = v_{T,y}^a$ and $v_{R,x}^a(t) = v_{R,x}^a, v_{R,y}^a(t) = v_{T,y}^a$.

Moreover, if the values of the accelerations $v_{T,x}^a, v_{T,y}^a, v_{R,x}^a$, and $v_{R,y}^a$ are appropriately selected, Case II can also model the scenario of time-varying speeds but with constant directions.

Case III: M2M with constant velocities The MT and MR do not experience velocity variations but move at particular speeds and directions. This can be derived by setting the accelerations of the MT and MR as zeros, that is, $v_{T,x}^a(t) = v_{T,y}^a(t) = 0$ and $v_{R,x}^a(t) = v_{R,y}^a(t) = 0$.

Case IV: F2M or mobile to fixed (M2F) The MT is stationary but MR moves at a constant speed and direction, or vice versa, that is, fixed base station to mobile vehicles or mobile vehicles to roadside infrastructures [5]. This can be derived by setting the velocity of MT (MR) to zero and that of MR (MT) as a constant value, that is, $v_{T,x}(t) = v_{T,y}(t) = 0$ and $v_{R,x}(t) = v_{R,x}, v_{R,y}(t) = v_{R,y}$ for F2M, while $v_{T,x}(t) = v_{T,x}, v_{T,y}(t) = v_{T,y}$ and $v_{R,x}(t) = v_{R,y}(t) = 0$ for M2F.

Case V: F2F The MT and MR are both stationary. In this scenario, the MT and MR can be viewed as two parked or slowly moving vehicles [4]. This can be derived by setting the velocities of MT and MR as zero, that is, $v_{T,x}(t) = v_{T,y}(t) = 0$ and $v_{R,x}(t) = v_{R,y}(t) = 0$.

B. Performance Analysis

Figure 4(a) shows the spatial CCFs of the proposed channel model for different time instants. It can be seen that as the normalized antenna element spacing δ_R/λ gradually increases, the absolute values of the spatial CCF show a decreasing trend, which conforms with the results in [49]. Furthermore, the fluctuations of the spatial CCFs gradually become slower as time increases. In Fig. 4(b), we note that the spatial CCFs exhibit different non-stationarity under different moving scenarios.

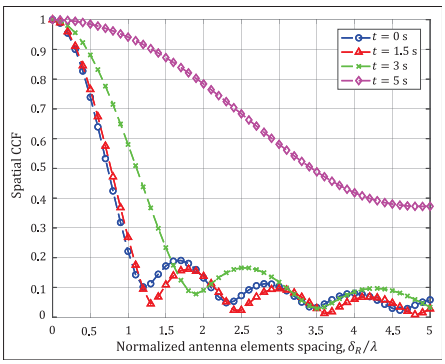

(a) Spatial CCFs at different times

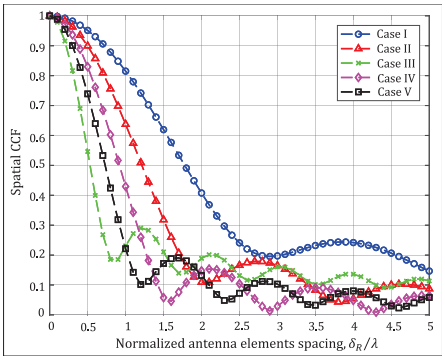

(b) Spatial CCFs in different scenarios, $t = 4$ s

Fig. 4. Spatial CCFs of the proposed channel model. (a) Case I, $v_{T,x}(0) = 5\ m/s$, $v_{T,y}(0) = -5\ m/s$, $v_{T,x}^a(0) = -3\ m/s^2$, $v_{T,y}^a(0) = -2\ m/s^2$, $v_{T,x}^{a2} = 2\ m/s^3$, $v_{T,y}^{a2} = -2\ m/s^3$ for MT, and $v_{R,x}(0) = 10\ m/s$, $v_{R,y}(0) = 10\ m/s$, $v_{R,x}^a(0) = 4\ m/s^2$, $v_{R,y}^a(0) = -4\ m/s^2$, $v_{R,x}^{a2} = 2\ m/s^3$, $v_{R,y}^{a2} = 2\ m/s^3$ for MR. (b) For Case I: the same as (a); for Case II: $v_{T,x}(0) = 5\ m/s$, $v_{T,y}(0) = -5\ m/s$, $v_{T,x}^a(0) = -3\ m/s^2$, $v_{T,y}^a(0) = -3\ m/s^2$ for MT, and $v_{R,x}(0) = 10\ m/s$, $v_{R,y}(0) = 5\ m/s$, $v_{R,x}^a(0) = 4\ m/s^2$, $v_{R,y}^a(0) = -4\ m/s^2$ for MR; for Case III: $v_{T,x}(0) = 5\ m/s$, $v_{T,y}(0) = 5\ m/s$ for MT, and $v_{R,x}(0) = -8\ m/s$, $v_{R,y}(0) = 8\ m/s$ for MR; for Case IV: fixed MT, and $v_{R,x}(t) = 10\ m/s$, $v_{R,y}(t) = 5\ m/s$ for MR; for Case V: fixed MT and MR.

Figure 5(a) shows the absolute values of the normalized FCF of the proposed multi-mobility V2X channel model at different times t. We can observe that the absolute values of the normalized FCF gradually decrease and then experience fluctuations when the frequency separation Δf increases, which is in agreement with the results in [13]. We can also see that as the moving time t increases, the normalized FCFs vary more rapidly. These results can be interpreted by the fact that, as the moving time t increases, the total propagation path lengths increase under the investigated moving conditions; hence, a small change in frequency separation Δf can result in large values of $\Delta f \tau_\ell(t)$, which makes the FCFs vary rapidly. Furthermore, under the investigated moving scenarios, Fig. 5(a) indicates that the coherence bandwidth of the proposed channel model is approximately 3 MHz

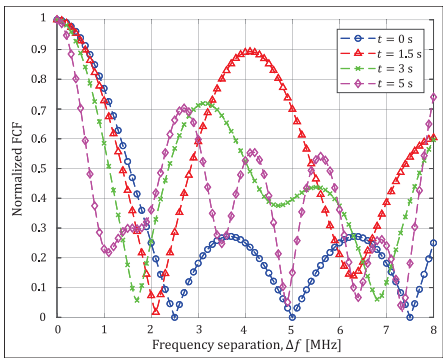

(a) FCFs at different times, $L = 4$

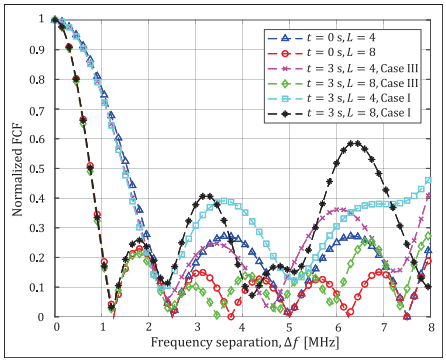

(b) FCFs for different time and cluster numbers

Fig. 5. FCFs of the proposed channel model. (a) Case I: $v_{T,x}(0) = 5\ m/s$, $v_{T,y}(0) = -5\ m/s$, $v^a_{T,x}(0) = v^a_{T,y}(0) = 1\ m/s^2$, $v^{a2}_{T,x} = v^{a2}_{T,y} = 1\ m/s^3$ for the MT; and $v_{R,x}(0) = 5\ m/s$, $v_{R,y}(0) = 5\ m/s$, $v^a_{R,x}(0) = v^a_{R,y}(0) = 1\ m/s^2$, $v^{a2}_{R,x} = v^{a2}_{R,y} = 1\ m/s^3$ for the MR. (b) For Case I: $v_{T,x}(0) = 5\ m/s$, $v_{T,y}(0) = -5\ m/s$, $v^a_{T,x}(0) = -1\ m/s^2$, $v^a_{T,y}(0) = -1\ m/s^2$, $v^{a2}_{T,x} = 1\ m/s^3$, $v^{a2}_{T,y} = -1\ m/s^3$ for MT, and $v_{R,x}(0) = -5\ m/s$, $v_{R,y}(0) = -5\ m/s$, $v^a_{R,x}(0) = 2\ m/s^2$, $v^a_{R,y}(0) = -2\ m/s^2$, $v^{a2}_{R,x} = -1\ m/s^3$, $v^{a2}_{R,y} = -1\ m/s^3$ for MR; for Case III: $v_{T,x}(t) = 4\ m/s$, $v_{T,y}(t) = -8\ m/s$ for MT, and $v_{R,x}(t) = -6\ m/s$, $v_{R,y}(t) = 4\ m/s$ for MR.

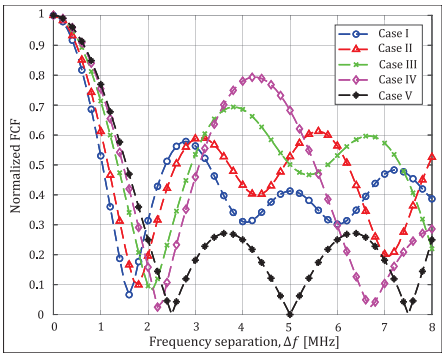

Fig. 6. FCFs of the proposed channel model with the same complex channel gains χ_ℓ under different moving scenarios, $L = 4$, $t = 4$ s, for Case I: $v_{T,x}(0) = 5\ m/s$, $v_{T,y}(0) = -5\ m/s$, $v^a_{T,x}(0) = -2\ m/s^2$, $v^a_{T,y}(0) = -4\ m/s^2$, $v^{a2}_{T,x} = 2\ m/s^3$, $v^{a2}_{T,y} = -2\ m/s^3$ for MT, and $v_{R,x}(0) = 10\ m/s$, $v_{R,y}(0) = 10\ m/s$, $v^a_{R,x}(0) = 2\ m/s^2$, $v^a_{R,y}(0) = -3\ m/s^2$, $v^{a2}_{R,x} = -2\ m/s^3$, $v^{a2}_{R,y} = -2\ m/s^3$ for MR; for Case II: $v_{T,x}(0) = 5\ m/s$, $v_{T,y}(0) = -5\ m/s$, $v^a_{T,x}(t) = -3\ m/s^2$, $v^a_{T,y}(t) = -3\ m/s^2$ for MT, and $v_{R,x}(0) = 10\ m/s$, $v_{R,y}(0) = 5\ m/s$, $v^a_{R,x}(t) = 4\ m/s^2$, $v^a_{R,y}(t) = -4\ m/s^2$ for MR; for Case III: $v_{T,x}(t) = 6\ m/s$, $v_{T,y}(t) = -3\ m/s$ for MT, and $v_{R,x}(t) = -3\ m/s$, $v_{R,y}(t) = 4\ m/s$ for MR; for Case IV: fixed MT, and $v_{R,x}(t) = 4\ m/s$, $v_{R,y}(t) = 1\ m/s$ for MR; for Case V: fixed MT and MR.

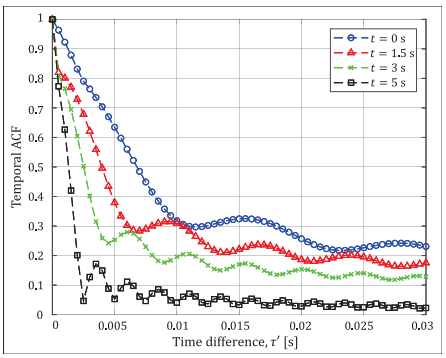

Fig. 7. Temporal ACFs of the proposed channel, where $\omega_\ell = 0.01$, $v_{T,x}(0) = 2\ m/s$, $v_{T,y}(0) = -2\ m/s$, $v^a_{T,x}(0) = 1\ m/s^2$, $v^a_{T,y}(0) = -1\ m/s^2$, $v^{a2}_{T,x} = -1\ m/s^3$, $v^{a2}_{T,y} = 1\ m/s^3$ for MT, and $v_{R,x}(0) = -2\ m/s$, $v_{R,y}(0) = 2\ m/s$, $v^a_{R,x}(0) = -1\ m/s^2$, $v^a_{R,y}(0) = 1\ m/s^2$, $v^{a2}_{R,x} = 1\ m/s^3$, $v^{a2}_{R,y} = 1\ m/s^3$ for MR.

when $t = 0$ s and reduces to approximately 1.2 MHz when $t = 5$ s as the threshold FCF value is set to be 0.5. The time-varying property of the coherence bandwidth of the channel also reveals the non-stationarity of the proposed V2X channel model, thus validating the effectiveness of the model. In Fig. 5(b), we observe that when the cluster number L increases, the channel decorrelates faster as the frequency separation Δf increases and the channel shows more rapid fluctuations. In Fig. 6, we observe that different movements of the mobile terminals can have different impacts on the channel frequency correlation properties.

By setting $\Delta p = \Delta q = 0$ in (33), the temporal ACFs of the proposed channel model for different time differences τ' are illustrated in Fig. 7. It should be noted that the temporal ACFs decrease as the time difference τ' increases gradually. Moreover, we can see that the temporal correlations of the proposed channel model decorrelate faster with the time difference τ' when the time t is larger, which is consistent with the results in [36]. Therefore, the temporal ACF of the proposed channel model is also related to the moving time t, which implies that the WSS assumption adopted in conventional stationary V2V channel models is no longer valid; thus, the non-stationarity of the proposed multi-mobility channel model is validated [37].

The non-stationarity of the proposed channel model is also investigated in Figure 8. From Fig. 8(a), we observe that the temporal correlation decreases faster with time, as the channel involves more dynamics. It should be noted that the temporal ACF in Case V, that is, the scenario of F2F, is a constant value and is independent of the time difference τ'. This phenomenon can be interpreted by the random motion of clusters. In Fig. 8(b), we notice that an increase in ω_ℓ can result in a decrease in temporal correlations. It is worth mentioning that the results in Figs. 7 and 8 reveal that there is a sharp transition for the temporal ACF from $\tau' = 0$ to $\tau' \neq 0$. As shown in (43), we can observe that $\varphi_{D,\ell,n}(t) - \varphi_{D,\ell,n}(t + \tau')$ equals zero when the time difference $\tau' = 0$, while for $\tau' \neq 0$, $\varphi_{D,\ell,n}(t)$ and $\varphi_{D,\ell,n}(t + \tau')$ are two independent Gaussian variables. Therefore, the transition occurs when $\tau' \neq 0$ because of the randomness of the independent phases $\varphi_{D,\ell,n}(t)$ and

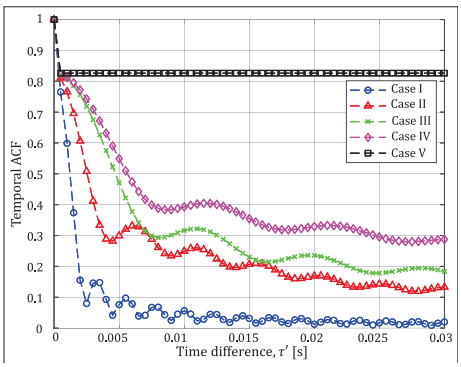

(a) ACFs in different scenarios, $t = 2$ s and $\omega_\ell = 0.01$

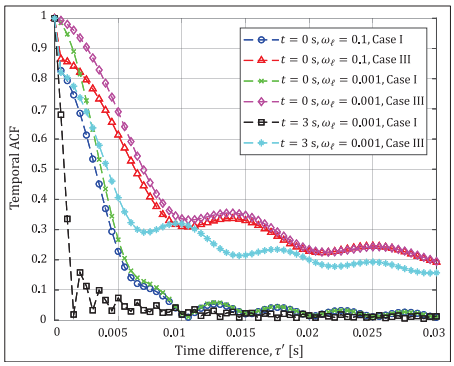

(b) ACFs for different time and cluster numbers

Fig. 8. Temporal ACFs of the proposed channel model. (a) For Case I: $v_{T,x}(0) = 5\ m/s$, $v_{T,y}(0) = 5\ m/s$, $v^a_{T,x}(0) = -3\ m/s^2$, $v^a_{T,y}(0) = -2\ m/s^2$, $v^{a2}_{T,x} = 2\ m/s^3$, $v^{a2}_{T,y} = -2\ m/s^3$ for MT, and $v_{R,x}(0) = 5\ m/s$, $v_{R,y}(0) = -5\ m/s$, $v^a_{R,x}(0) = 4\ m/s^2$, $v^a_{R,y}(0) = -4\ m/s^2$, $v^{a2}_{R,x} = 2\ m/s^3$, $v^{a2}_{R,y} = 2\ m/s^3$ for MR; for Case II: $v_{T,x}(0) = 8\ m/s$, $v_{T,y}(0) = -4\ m/s$, $v^a_{T,x}(t) = -4\ m/s^2$, $v^a_{T,y}(t) = -5\ m/s^2$ for MT, and $v_{R,x}(0) = -5\ m/s$, $v_{R,y}(0) = 5\ m/s$, $v^a_{R,x}(t) = 4\ m/s^2$, $v^a_{R,y}(t) = -4\ m/s^2$ for MR; for Case III: $v_{T,x}(t) = 4\ m/s$, $v_{T,y}(t) = 6\ m/s$ for MT, and $v_{R,x}(t) = -5\ m/s$, $v_{R,y}(t) = 5\ m/s$ for MR; for Case IV: fixed MT, and $v_{R,x}(t) = -5\ m/s$, $v_{R,y}(t) = 5\ m/s$ for MR; for Case V: fixed MT and MR. (b) Parameters for Cases I and III are the same as Fig. 8(a).

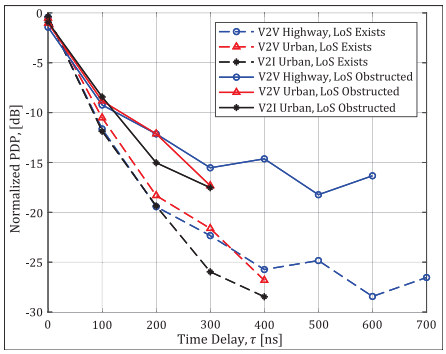

Fig. 9. Normalized PDP of the proposed V2X channel model in different communication scenarios.

$\varphi_{D,\ell,n}(t + \tau')$, which is the same result that was obtained for Case V in Fig. 8(a).

By using (47), Fig. 9 illustrates the normalized PDPs of the proposed V2X channel model in different communication scenarios, such as V2V on a highway, V2V in urban streets, and V2I in urban streets, which are typical V2X communication scenarios [1]. It can be seen that in different scenarios, the PDPs of the proposed channel model show different properties; generally, the PDPs show higher values in the dense scattering scenario (V2V Urban) as compared to relatively nondense scattering scenario (V2I Urban) [50]. Moreover, we compared the PDPs of the proposed channel model for the scenario with existing and obstructed LoS. It can be seen that when the LoS path is obstructed, the normalized PDPs of multipath components are more comparable with respect to the first path. In contrast, when the LoS path exists, the power is more centered in the first path, which conforms with the results in [15].

V. Conclusion

This paper has proposed a novel general multi-mobility MIMO GBSM for future intelligent V2X channels, which can capture the non-stationarity caused by the velocity and trajectory variations of the terminals and random motion of the clusters, making it more applicable to realistic scenarios than existing models. The proposed modeling solution can provide a general and accurate description of the physical propagation characteristics of realistic V2X channels, which can help researchers to conduct physical and network layer algorithm validations and system performance analyses via simulations. The results demonstrate that the Doppler phase is a Gaussian random process with time-varying mean value and variance under the assumption of the random walk of the clusters. Based on the non-isotropic scattering assumption, important statistical properties of the proposed channel model, such as spatial CCF, temporal ACF, FCF, and PDP, have been derived and thoroughly investigated. The results revealed that the temporal correlation of the channel decreases faster with time when the channel involves more dynamics. Furthermore, they can also inform the design of the system level transmission scheme, such as transmission bandwidth and symbol duration. Finally, the agreement between the simulation and measurement results validates the effectiveness of the proposed model. In a future study, the birth and death of clusters will be considered. Moreover, we aim to conduct measurements in realistic V2X scenarios to further validate the proposed non-WSS channel model.

Appendix I

Owing to the nonlinear nature of the angles $\alpha_{T,\ell,n}(t)$ and $\alpha_{R,\ell,n}(t)$, it is impossible to obtain the analytic results of $\mu_{\varphi_{D,\ell,n}}(t)$ and $\sigma^2_{\varphi_{D,\ell,n}}(t)$ by directly substituting (23) and (24) into (30) and (31). Therefore, we need to represent the sine and cosine of the time-varying angles as linear polynomials of time t by a Taylor series expansion. Let us take the time-varying AoD as an example. The sine and cosine values of $\alpha_{T,\ell,n}(t)$ can be expressed as (48) and (49), respectively, as shown at the bottom of the next page.

Let $g(t) = \Big[\big(D_{T,\ell,n}(0)\cos\alpha_{T,\ell,n}(0) - r^x_T(t)\big)^2 + \big(D_{T,\ell,n}(0)\sin\alpha_{T,\ell,n}(0) - r^y_T(t)\big)^2\Big]^{-\frac{1}{2}}$, based on the results in (11) and (12), and by extracting the factor $1/D_{T,\ell,n}(0)$, we can express $g(t)$ as (50), as shown at the bottom of the next page. Then, let $g(t) = \frac{1}{D_{T,\ell,n}(0)}\big[1 + A(t)\big]^{-\frac{1}{2}}$ and $A(t) = -k_1\ t - k_2\ t^2 - k_3\ t^3 + k_4\ t^4 + k_5\ t^5 + k_6\ t^6$. It should be noted

that the propagation path length $D_{T,\ell,n}(0)$ is generally on the order of 10^2 m in practice, while the motion parameters $v_{T,x}(0), v_{T,y}(0), v^a_{T,x}(0), v^a_{T,y}(0), v^{a2}_{T,x}$, and $v^{a2}_{T,y}$, etc., are much smaller than $D_{T,\ell,n}(0)$; consequently, the coefficients $\{k_4, k_5, k_6\}$ are much smaller than $\{k_1, k_2, k_3\}$ and hence can be neglected. Moreover, by taking the observation time t as a small value, i.e., several seconds, we find that $A(t)$ is smaller than 1. Therefore, $g(t)$ in (50) can be approximated by its first-order Taylor series expansions as

$$\begin{aligned} & g(t) \\ & \approx \big(1-0.5A(t)\big)/D_{T,\ell,n}(0) \\ & \approx \underbrace{\frac{1}{D_{T,\ell,n}(0)}}_{o_{10}} + \underbrace{\frac{\cos\alpha_{T,\ell,n}(0)v_{T,x}(0)+\sin\alpha_{T,\ell,n}(0)v_{T,y}(0)}{D^2_{T,\ell,n}(0)}}_{o_{11}} t \\ & \quad + \underbrace{\frac{\cos\alpha_{T,\ell,n}(0)v^a_{T,x}(0)+\sin\alpha_{T,\ell,n}(0)v^a_{T,y}(0)}{2D^2_{T,\ell,n}(0)}}_{o_{12}} t^2 \\ & \quad + \underbrace{\frac{\cos\alpha_{T,\ell,n}(0)v^{a2}_{T,x}+\sin\alpha_{T,\ell,n}(0)v^{a2}_{T,y}}{6D^2_{T,\ell,n}(0)}}_{o_{13}} t^3. \end{aligned} \tag{51}$$

Similarly, for the sine and cosine of the time-varying AoA $\alpha_{R,\ell,n}(t)$ in (24), we can obtain the approximation in (52), shown at the top of the next page, where the coefficients $\{o_{20}, o_{21}, o_{22}, o_{23}\}$ have the same form as $\{o_{10}, o_{11}, o_{12}, o_{13}\}$ in (51) only with the subscript T of the parameters replaced by R.

Therefore, based on the results from (11) and (51), we can approximate (48) as (53), as shown at the top of the next page. Similarly, we have the following approximations:

$$\begin{aligned} & \sin\alpha_{T,\ell,n}(t) \\ & \approx P_{20}+P_{21}t+P_{22}t^2+P_{23}t^3+P_{24}t^4+P_{25}t^5+P_{26}t^6, \end{aligned} \tag{54}$$

$$\begin{aligned} & \cos\alpha_{R\ell,n}(t) \\ & \approx Q_{10}+Q_{11}t+Q_{12}t^2+Q_{13}t^3+Q_{14}t^4+Q_{15}t^5+Q_{16}t^6, \end{aligned} \tag{55}$$

$$\begin{aligned} & \sin\alpha_{R,\ell,n}(t) \\ & \approx Q_{20}+Q_{21}t+Q_{22}t^2+Q_{23}t^3+Q_{24}t^4+Q_{25}t^5+Q_{26}t^6, \end{aligned} \tag{56}$$

By substituting (7)-(10) and (53)-(56) into (30), the closed-form solution to the time-varying mean value $\mu_{\varphi_{D,\ell,n}}(t)$ can be approximated as

$$\begin{aligned} & \mu_{\varphi_{D,\ell,n}}(t) \\ & \approx \frac{2\pi}{\lambda}\Big[\big(b_{10}+b_{20}+d_{10}+d_{20}\big)t \\ & \quad +\frac{1}{2}\big(b_{11}+b_{21}+d_{11}+d_{21}\big)t^2+\frac{1}{3}\big(b_{12}+b_{22}+d_{12}+d_{22}\big)t^3 \\ & \quad +\frac{1}{4}\big(b_{13}+b_{23}+d_{13}+d_{23}\big)t^4+\frac{1}{5}\big(b_{14}+b_{24}+d_{14}+d_{24}\big)t^5 \end{aligned}$$

$$\cos\alpha_{T,\ell,n}(t)=\frac{D_{T,\ell,n}(0)\cos\alpha_{T,\ell,n}(0)-r^x_T(t)}{\sqrt{\big(D_{T,\ell,n}(0)\cos\alpha_{T,\ell,n}(0)-r^x_T(t)\big)^2+\big(D_{T,\ell,n}(0)\sin\alpha_{T,\ell,n}(0)-r^y_T(t)\big)^2}}, \tag{48}$$

$$\sin\alpha_{T,\ell,n}(t)=\frac{D_{T,\ell,n}(0)\sin\alpha_{T,\ell,n}(0)-r^y_T(t)}{\sqrt{\big(D_{T,\ell,n}(0)\cos\alpha_{T,\ell,n}(0)-r^x_T(t)\big)^2+\big(D_{T,\ell,n}(0)\sin\alpha_{T,\ell,n}(0)-r^y_T(t)\big)^2}}. \tag{49}$$

$$\begin{aligned} & g(t) \\ & =\frac{1}{D_{T,\ell,n}(0)}\Bigg\{1-\underbrace{\frac{2\cos\alpha_{T,\ell,n}(0)v_{T,x}(0)+2\sin\alpha_{T,\ell,n}(0)v_{T,y}(0)}{D_{T,\ell,n}(0)}}_{k_1}t \\ & \quad -\underbrace{\Big(\frac{\cos\alpha_{T,\ell,n}(0)v^a_{T,x}(0)}{D_{T,\ell,n}(0)}+\frac{\sin\alpha_{T,\ell,n}(0)v^a_{T,y}(0)}{D_{T,\ell,n}(0)}-\frac{v^2_{T,x}(0)}{D^2_{T,\ell,n}(0)}-\frac{v^2_{T,y}(0)}{D^2_{T,\ell,n}(0)}\Big)}_{k_2}t^2 \\ & \quad -\underbrace{\Big(\frac{\cos\alpha_{T,\ell,n}(0)v^{a2}_{T,x}}{3D_{T,\ell,n}(0)}+\frac{\sin\alpha_{T,\ell,n}(0)v^{a2}_{T,y}}{3D_{T,\ell,n}(0)}-\frac{v_{T,x}(0)v^a_{T,x}(0)}{D^2_{T,\ell,n}(0)}-\frac{v_{T,y}(0)v^a_{T,y}(0)}{D^2_{T,\ell,n}(0)}\Big)}_{k_3}t^3 \\ & \quad +\underbrace{\Big(\frac{(v^a_{T,x}(0))^2}{4D^2_{T,\ell,n}(0)}+\frac{v_{T,x}(0)v^{a2}_{T,x}}{3D^2_{T,\ell,n}(0)}+\frac{(v^a_{T,y}(0))^2}{4D^2_{T,\ell,n}(0)}+\frac{v_{T,y}(0)v^{a2}_{T,y}}{3D^2_{T,\ell,n}(0)}\Big)}_{k_4}t^4+\underbrace{\frac{v^a_{T,x}(0)v^{a2}_{T,x}+v^a_{T,y}(0)v^{a2}_{T,y}}{6D^2_{T,\ell,n}(0)}}_{k_5}t^5+\underbrace{\frac{(v^{a2}_{T,x})^2+(v^{a2}_{T,y})^2}{36D^2_{T,\ell,n}(0)}}_{k_6}t^6\Bigg\}^{-\frac{1}{2}}. \end{aligned} \tag{50}$$

$$\begin{aligned}
&\Big[\big(D_{R,\ell,n}(0)\cos\alpha_{R,\ell,n}(0)-r_R^x(t)\big)^2+\big(D_{R,\ell,n}(0)\sin\alpha_{R,\ell,n}(0)-r_R^y(t)\big)^2\Big]^{-1/2}\\
&\quad\approx o_{20}+o_{21}t+o_{22}t^2+o_{23}t^3, \qquad (52)\\
&\cos\alpha_{T,\ell,n}(t)\approx\big(D_{T,\ell,n}(0)\cos\alpha_{T,\ell,n}(0)-r_T^x(t)\big)(o_{10}+o_{11}t+o_{12}t^2+o_{13}t^3)\\
&\quad=\underbrace{D_{T,\ell,n}(0)\cos\alpha_{T,\ell,n}(0)o_{10}}_{P_{10}}+\underbrace{\big(D_{T,\ell,n}(0)\cos\alpha_{T,\ell,n}(0)o_{11}-v_{T,x}(0)o_{10}\big)}_{P_{11}}t\\
&\qquad+\underbrace{\big(D_{T,\ell,n}(0)\cos\alpha_{T,\ell,n}(0)o_{12}-v_{T,x}(0)o_{11}-\frac{1}{2}v_{T,x}^a(0)o_{10}\big)}_{P_{12}}t^2\\
&\qquad+\underbrace{\big(D_{T,\ell,n}(0)\cos\alpha_{T,\ell,n}(0)o_{13}-v_{T,x}(0)o_{12}-\frac{1}{2}v_{T,x}^a(0)o_{11}-\frac{1}{6}v_{T,x}^{a2}o_{10}\big)}_{P_{13}}t^3\\
&\qquad-\underbrace{\big(v_{T,x}(0)o_{13}+\frac{1}{2}v_{T,x}^a(0)o_{12}+\frac{1}{6}v_{T,x}^{a2}o_{11}\big)}_{P_{14}}t^4-\underbrace{\big(\frac{1}{2}v_{T,x}^a(0)o_{13}+\frac{1}{6}v_{T,x}^{a2}o_{12}\big)}_{P_{15}}t^5-\underbrace{\frac{1}{6}v_{T,x}^{a2}o_{13}}_{P_{16}}t^6. \qquad (53)
\end{aligned}$$

$$\begin{aligned}
&+\frac{1}{6}\big(b_{15}+b_{25}+d_{15}+d_{25}\big)t^6+\frac{1}{7}\big(b_{16}+b_{26}+d_{16}+d_{26}\big)t^7\\
&+\frac{1}{8}\big(b_{17}+b_{27}+d_{17}+d_{27}\big)t^8+\frac{1}{9}\big(b_{18}+b_{28}+d_{18}+d_{28}\big)t^9\Big], \qquad (57)
\end{aligned}$$

where the coefficients $\{b_{10}, b_{11}, \cdots, b_{18}\}$ are constant parameters, which can be expressed as $b_{10} = P_{10}v_{T,x}(0)$, $b_{11} = P_{11}v_{T,x}(0) + P_{10}v_{T,x}^a(0)$, $b_{12} = P_{12}v_{T,x}(0) + P_{11}v_{T,x}^a(0) + P_{10}v_{T,x}^{a2}/2$, $b_{13} = P_{13}v_{T,x}(0) + P_{12}v_{T,x}^a(0) + P_{11}v_{T,x}^{a2}/2$, $b_{14} = P_{14}v_{T,x}(0) + P_{13}v_{T,x}^a(0) + P_{12}v_{T,x}^{a2}/2$, $b_{15} = P_{15}v_{T,x}(0) + P_{14}v_{T,x}^a(0) + P_{13}v_{T,x}^{a2}/2$, $b_{16} = P_{16}v_{T,x}(0) + P_{15}v_{T,x}^a(0) + P_{14}v_{T,x}^{a2}/2$, $b_{17} = P_{16}v_{T,x}^a(0) + P_{15}v_{T,x}^{a2}/2$, and $b_{18} = P_{16}v_{T,x}^{a2}/2$, respectively. Moreover, other coefficients in (57), such as $\{b_{20}, \cdots, b_{28}\}$, $\{d_{10}, \cdots, d_{18}\}$, and $\{d_{20}, \cdots, d_{28}\}$, can be derived in a similar way.

By substituting (53)-(56) into (31), we can obtain the approximated closed-form solution to the time-varying variance $\sigma^2_{\varphi_{D,\ell,n}}(t)$ of the random phase $\varphi_{D,\ell,n}(t)$ as

$$\begin{aligned}
&\sigma^2_{\varphi_{D,\ell,n}}(t)\\
&\approx \frac{8\pi^2}{\lambda^2}\omega_{\ell,c}t+\frac{8\pi^2}{\lambda^2}\omega_{\ell,c}\Big\{(u_0+v_0)t+\frac{1}{2}(u_1+v_1)t^2\\
&\quad+\frac{1}{3}(u_2+v_2)t^3+\frac{1}{4}(u_3+v_3)t^4+\frac{1}{5}(u_4+v_4)t^5\\
&\quad+\frac{1}{6}(u_5+v_5)t^6+\frac{1}{7}(u_6+v_6)t^7+\frac{1}{8}(u_7+v_7)t^8\\
&\quad+\frac{1}{9}(u_8+v_8)t^9+\frac{1}{10}(u_9+v_9)t^{10}+\frac{1}{11}(u_{10}+v_{10})t^{11}\\
&\quad+\frac{1}{12}(u_{11}+v_{11})t^{12}+\frac{1}{13}(u_{12}+v_{12})t^{13}\Big\}, \qquad (58)
\end{aligned}$$

where coefficients $\{u_0, u_1, \cdots, u_{12}\}$ are constant parameters, and they can be expressed as $u_0 = P_{10}Q_{10}$, $u_1 = P_{10}Q_{11} + P_{11}Q_{10}$, $u_2 = P_{10}Q_{12} + P_{11}Q_{11} + P_{12}Q_{10}$, $u_3 = P_{10}Q_{13} + P_{11}Q_{12} + P_{12}Q_{11} + P_{13}Q_{10}$, $u_4 = P_{10}Q_{14} + P_{11}Q_{13} + P_{12}Q_{12} + P_{13}Q_{11} + P_{14}Q_{10}$, $u_5 = P_{10}Q_{15} + P_{11}Q_{14} + P_{12}Q_{13} + P_{13}Q_{12} + P_{14}Q_{11} + P_{15}Q_{10}$, $u_6 = P_{10}Q_{16} + P_{11}Q_{15} + P_{12}Q_{14} + P_{13}Q_{13} + P_{14}Q_{12} + P_{15}Q_{11} + P_{16}Q_{10}$, $u_7 = P_{11}Q_{16} + P_{16}Q_{11}$, $u_8 = P_{12}Q_{16} + P_{16}Q_{12}$, $u_9 = P_{13}Q_{16} + P_{16}Q_{13}$, $u_{10} = P_{14}Q_{16} + P_{16}Q_{14}$, $u_{11} = P_{15}Q_{16} + P_{16}Q_{15}$, and $u_{12} = P_{16}Q_{16} + P_{16}Q_{16}$, respectively. Finally, other coefficients in (58), that is, $\{v_0, v_1, \cdots, v_{12}\}$, can be derived in a similar manner. We omit them here for brevity.

REFERENCES

[1] X. Cheng, R. Q. Zhang, and L. Q. Yang, *5G-Enabled Vehicular Communications and Networking*. Cham, Switzerland: Springer, 2019.

[2] K. Wevers and M. Lu, "V2X communication for ITS-from IEEE 802.11 p towards 5G," *IEEE 5G Tech. Focus*, vol. 1, no. 2, pp. 5–10, Jun. 2017.

[3] X. Cheng, C. Chen, W. Zhang, and Y. Yang, "5G-enabled cooperative intelligent vehicular (5GenCIV) framework: When benz meets marconi," *IEEE Intell. Syst.*, vol. 32, no. 3, pp. 53–59, May 2017.

[4] S. Thoen, L. Van der Perre, and M. Engels, "Modeling the channel time-variance for fixed wireless communications," *IEEE Commun. Lett.*, vol. 6, no. 8, pp. 331–333, Aug. 2002.

[5] G. Makhoul, F. Mani, R. DErrico, and C. Oestges, "On the modeling of time correlation functions for mobile-to-mobile fading channels in indoor environments," *IEEE Antennas Wireless Propag. Lett.*, vol. 16, pp. 549–552, Mar. 2017.

[6] R. He *et al.*, "Propagation channels of 5G millimeter-wave vehicle-to-vehicle communications: Recent advances and future challenges," *IEEE Veh. Technol. Mag.*, vol. 15, no. 1, pp. 16–26, Mar. 2020.

[7] C.-X. Wang, J. Bian, J. Sun, W. Zhang, and M. Zhang, "A survey of 5G channel measurements and models," *IEEE Commun. Surveys Tuts.*, vol. 20, no. 4, pp. 3142–3168, 4th Quart., 2018.

[8] W. Viriyasitavat, M. Boban, H.-M. Tsai, and A. Vasilakos, "Vehicular communications: Survey and challenges of channel and propagation models," *IEEE Veh. Technol. Mag.*, vol. 10, no. 2, pp. 55–66, Jun. 2015.

[9] C.-X. Wang, X. Cheng, and D. I. Laurenson, "Vehicle-to-vehicle channel modeling and measurements: Recent advances and future challenges," *IEEE Commun. Mag.*, vol. 47, no. 11, pp. 96–103, Nov. 2009.

[10] M. Yang *et al.*, "A cluster-based three-dimensional channel model for vehicle-to-vehicle communications," *IEEE Trans. Veh. Technol.*, vol. 68, no. 6, pp. 5208–5220, Jun. 2019.

[11] J. Maurer, T. Fugen, M. Porebska, T. Zwick, and W. Wisebeck, "A ray-optical channel model for mobile to mobile communications," in *Proc. 4th MCM COST 2100*, Wroclaw, Poland, Feb. 2008.

[12] X. Zhao, X. Liang, S. Li, and B. Ai, "Two-cylinder and multi-ring GBSSM for realizing and modeling of vehicle-to-vehicle wideband MIMO channels," *IEEE Trans. Intell. Transp. Syst.*, vol. 17, no. 10, pp. 2787–2799, Oct. 2016.

[13] S. Wu, C.-X. Wang, H. Haas, E.-H.-M. Aggoune, M. M. Alwakeel, and B. Ai, "A non-stationary wideband channel model for massive MIMO communication systems," *IEEE Trans. Wireless Commun.*, vol. 14, no. 3, pp. 1434–1446, Mar. 2015.
[14] Y. Li, B. Ai, X. Cheng, S. Lin, and Z. Zhong, "A TDL based non-WSSUS vehicle-to-vehicle channel model," *Int. J. Antennas Propag.*, vol. 2013, pp. 1–8, 2013.
[15] Z. Huang, X. Zhang, and X. Cheng, "Non-geometrical stochastic model for non-stationary wideband vehicular communication channels," *IET Commun.*, vol. 14, no. 1, pp. 54–62, Jan. 2020.
[16] *Technical Specification Group Radio Access Network; Study on 3D Channel Model for LTE (Release 12)*, document TR 36.873, v12.2.0, 3GPP, Jun. 2015.
[17] *Technical Specification Group Radio Access Network; Study on Channel Model for Frequencies from 0.5 to 100 GHz (Release 16)*, document TR 38.901, v16.1.0, 3GPP, Dec. 2019.
[18] P. Kyosti *et al.*, *WINNER II Channel Models*, document IST-4-027756 WINNER II, D.1.1.2, v1.0, Sep. 2007.
[19] *Guidelines for Evaluation of Radio Interface Technologies for IMT Advanced*, document ITU-R M.2135-1, Dec. 2009.
[20] J. Karedal *et al.*, "Measurement-based modeling of vehicle-to-vehicle MIMO channels," in *Proc. IEEE Int. Conf. Commun.*, Dresden, Germany, Jun. 2009, pp. 1–6.
[21] Q. Zhu *et al.*, "A novel 3D non-stationary wireless MIMO channel simulator and hardware emulator," *IEEE Trans. Commun.*, vol. 66, no. 9, pp. 3865–3878, Sep. 2018.
[22] A. Ispas, C. Schneider, G. Ascheid, and R. Thoma, "Analysis of the local quasi-stationarity of measured dual-polarized MIMO channels," *IEEE Trans. Veh. Technol.*, vol. 64, no. 8, pp. 3481–3493, Aug. 2015.
[23] R. He *et al.*, "Vehicle-to-vehicle radio channel characterization in crossroad scenarios," *IEEE Trans. Veh. Technol.*, vol. 65, no. 8, pp. 5850–5861, Aug. 2016.
[24] X. Cheng, Z. Huang, and S. Chen, "Vehicular communication channel measurement, modelling, and application for beyond 5G and 6G," *IET Commun.*, vol. 14, no. 19, pp. 3303–3311, Dec. 2020.
[25] X. Cheng, R. Zhang, and L. Yang, "Wireless towards the era of intelligent vehicles," *IEEE Internet Things J.*, vol. 6, no. 1, pp. 188–202, Feb. 2019.
[26] Y. Yuan, C.-X. Wang, Y. He, M. M. Alwakeel, and E.-H.-M. Aggoune, "3D wideband non-stationary geometry-based stochastic models for non-isotropic MIMO vehicle-to-vehicle channels," *IEEE Trans. Wireless Commun.*, vol. 14, no. 12, pp. 6883–6895, Dec. 2015.
[27] H. Jiang, Z. Zhang, L. Wu, J. Dang, and G. Gui, "A 3-D non-stationary wideband geometry-based channel model for MIMO vehicle-to-vehicle communications in tunnel environments," *IEEE Trans. Veh. Technol.*, vol. 68, no. 7, pp. 6257–6271, Jul. 2019.
[28] R. He, B. Ai, G. L. Stuber, G. Wang, and Z. Zhong, "Geometrical-based modeling for millimeter-wave MIMO mobile-to-mobile channels," *IEEE Trans. Veh. Technol.*, vol. 67, no. 4, pp. 2848–2863, Apr. 2018.
[29] A. Borhani and M. Patzold, "Correlation and spectral properties of vehicle-to-vehicle channels in the presence of moving scatterers," *IEEE Trans. Veh. Technol.*, vol. 62, no. 9, pp. 4228–4239, Nov. 2013.
[30] A. G. Zajic, "Impact of moving scatterers on vehicle-to-vehicle narrowband channel characteristics," *IEEE Trans. Veh. Technol.*, vol. 63, no. 7, pp. 3094–3106, Sep. 2014.
[31] A. Ghazal *et al.*, "A non-stationary IMT-advanced MIMO channel model for high-mobility wireless communication systems," *IEEE Trans. Wireless Commun.*, vol. 16, no. 4, pp. 2057–2068, Apr. 2017.
[32] R. Iqbal and T. D. Abhayapala, "Impact of mobile acceleration on the statistics of Rayleigh fading channel," in *Proc. 8th Austral. Commun. Theory Workshop (AusCTW)*, 2007, pp. 122–128.
[33] W. Li, X. Chen, Q. Zhu, W. Zhong, D. Xu, and F. Bai, "A novel segment-based model for non-stationary vehicle-to-vehicle channels with velocity variations," *IEEE Access*, vol. 7, pp. 133422–133451, Sep. 2019.
[34] M. Patzold and A. Borhani, "A non-stationary multipath fading channel model incorporating the effect of velocity variations of the mobile station," *IEEE Wireless Commun. Netw. Conf. (WCNC)*, Istanbul, Turkey, Apr. 2014, pp. 182–187.
[35] J. Bian, C.-X. Wang, M. Zhang, X. Ge, and X. Gao, "A 3-D non-stationary wideband MIMO channel model allowing for velocity variations of the mobile station," in *Proc. IEEE Int. Conf. Commun. (ICC)*, Paris, France, May 2017, pp. 21–25.
[36] W. Dahech, M. Patzold, C. A. Gutierrez, and N. Youssef, "A non-stationary mobile-to-mobile channel model allowing for velocity and trajectory variations of the mobile stations," *IEEE Trans. Wireless Commun.*, vol. 16, no. 3, pp. 1987–2000, Mar. 2017.
[37] Q. Zhu *et al.*, "Temporal correlations for a non-stationary vehicle-to-vehicle channel model allowing velocity variations," *IEEE Commun. Lett.*, vol. 23, no. 7, pp. 1280–1284, Jul. 2019.
[38] H. Jiang, Z. Zhang, J. Dang, and L. Wu, "Analysis of geometric multibounced virtual scattering channel model for dense urban street environments," *IEEE Trans. Veh. Technol.*, vol. 66, no. 3, pp. 1903–1912, Mar. 2017.
[39] H. Jiang, Z. Zhang, and G. Gui, "A novel estimated wideband geometry-based vehicle-to-vehicle channel model using an AoD and AoA estimation algorithm," *IEEE Access*, vol. 7, pp. 35124–35131, Feb. 2019.
[40] S. Wu, C.-X. Wang, E.-H.-M. Aggoune, M. M. Alwakeel, and X. You, "A general 3-D non-stationary 5G wireless channel model," *IEEE Trans. Commun.*, vol. 66, no. 7, pp. 3065–3078, Jul. 2018.
[41] J. Bian *et al.*, "A WINNER+ based 3-D non-stationary wideband MIMO channel model," *IEEE Trans. Wireless Commun.*, vol. 17, no. 3, pp. 1755–1767, Mar. 2018.
[42] Y. Liu, C.-X. Wang, and J. Huang, "Recent developments and future challenges in channel measurements and models for 5G and beyond high-speed train communication systems," *IEEE Commun. Mag.*, vol. 57, no. 9, pp. 50–56, Sep. 2019.
[43] A. Borhani and M. Ptzold, "Modeling of vehicle-to-vehicle channels in the presence of moving scatterers," in *Proc. IEEE Veh. Technol. Conf. (VTC Fall)*, Quebec City, QC, Canada, Sep. 2012, pp. 3–6.
[44] A. Borhani, G. L. Stuber, and M. Patzold, "A random trajectory approach for the development of nonstationary channel models capturing different scales of fading," *IEEE Trans. Veh. Technol.*, vol. 66, no. 1, pp. 1–13, Jan. 2017.
[45] R. He, B. Ai, G. L. Stuber, and Z. Zhong, "Mobility model-based non-stationary Mobile-to-Mobile channel modeling," *IEEE Trans. Wireless Commun.*, vol. 17, no. 7, pp. 4388–4400, Jul. 2018.
[46] L. Sanguinetti, A. L. Moustakas, E. Bjornson, and M. Debbah, "Large system analysis of the energy consumption distribution in multi-user MIMO systems with mobility," *IEEE Trans. Wireless Commun.*, vol. 14, no. 3, pp. 1730–1745, Mar. 2015.
[47] A. Goldsmith, *Wireless Communication*. Cambridge, U.K.: Cambridge Univ. Press, 2005.
[48] M. Patzold, *Mobile Radio Channels*, 2nd ed. West Sussex, U.K.: Wiley, 2005.
[49] S. Wu, C.-X. Wang, E.-H.-M. Aggoune, M. M. Alwakeel, and Y. He, "A non-stationary 3-D wideband twin-cluster model for 5G massive MIMO channels," *IEEE J. Sel. Areas Commun.*, vol. 32, no. 6, pp. 1207–1218, Jun. 2014.
[50] G. Acosta-Marum and M. A. Ingram, "Six time- and frequency- selective empirical channel models for vehicular wireless LANs," *IEEE Veh. Technol. Mag.*, vol. 2, no. 4, pp. 4–11, Dec. 2007.

Baiping Xiong received the B.Eng. degree in information engineering from Southeast University, Nanjing, China, in 2019, where he is currently pursuing the Ph.D. degree with the National Mobile Communications Research Laboratory.

Zaichen Zhang (Senior Member, IEEE) was born in Nanjing, China, in 1975. He received the B.S. and M.S. degrees in electrical and information engineering from Southeast University, Nanjing, in 1996 and 1999, respectively, and the Ph.D. degree in electrical and electronic engineering from The University of Hong Kong, Hong Kong, in 2002. From 2002 to 2004, he was a Post-Doctoral Fellow with the National Mobile Communications Research Laboratory, Southeast University. He joined the School of Information Science and Engineering, Southeast University, in 2004, where he is currently a Professor. He has published more than 200 articles and issued 50 patents. His current research interests include 6G mobile communication systems, optical wireless communications, and quantum information processing.

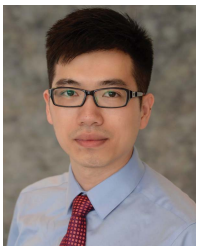

Jiangfan Zhang (Member, IEEE) received the B.Eng. degree in communication engineering from the Huazhong University of Science and Technology, Wuhan, China, in 2008, the M.Eng. degree in information and communication engineering from Zhejiang University, Hangzhou, China, 2011, and the Ph.D. degree in electrical engineering from Lehigh University, Bethlehem, PA, USA, in 2016. From 2016 to 2018, he was a Post-Doctoral Research Scientist with the Department of Electrical Engineering, Columbia University, New York, NY, USA. Since 2018, he has been with the Department of Electrical and Computer Engineering, Missouri University of Science and Technology, Rolla, MO, USA, where he is currently an Assistant Professor. His research interests include signal processing, machine learning, and their applications to cybersecurity, cyber-physical systems, the Internet of Things, smart grids, and sonar processing. He was a recipient of the Dean's Ph.D. Student Assistantship, a Gotshall Fellowship, and a P. C. Rossin Doctoral Fellow at Lehigh University.

Hao Jiang (Member, IEEE) received the B.S. and M.S. degrees in electrical and information engineering from the Nanjing University of Information Science and Technology, Nanjing, China, in 2012 and 2015, respectively, and the Ph.D. degree from Southeast University, Nanjing, in 2019. From 2017 to 2018, he was a Visiting Student with the Department of Electrical Engineering, Columbia University in the City of New York, New York, NY, USA. Since April 2019, he has been a Professor with the School of Information Science and Engineering, Nanjing University of Information Science and Technology. His current research interests include in the general area of wireless channel measurements and modeling, B5G wireless communication networks, signal processing, machine learning, and AI-driven technologies.

Jian Dang (Senior Member, IEEE) received the B.S. degree in information engineering and the Ph.D. degree in information and communications engineering from Southeast University, Nanjing, China, in July 2007 and September 2013, respectively. From September 2010 to March 2012, he was with the Department of Electrical and Computer Engineering, University of Florida, Gainesville, FL, USA, as a Visiting Scholar. Since September 2013, he has been with the National Mobile Communications Research Laboratory, Southeast University. He is currently an associate professor. His research interests include signal processing in wireless communications and optical mobile communications.

Liang Wu (Member, IEEE) received the B.S., M.S., and Ph.D. degrees all from School of Information Science and Engineering, Southeast University, Nanjing, China, in 2007, 2010, and 2013, respectively. From September 2011 to March 2013, he was with the School of Electrical Engineering and Computer Science, Oregon State University, as a Visiting Ph.D. Student. In September 2013, he joined the National Mobile Communications Research Laboratory, Southeast University, where he has been an Associate Professor, since April 2018. His research interests include optical wireless communications, multiple input and multiple output technology, interference alignment, and wireless indoor localization.